Supporting Information for:

Reactivity of the Copper(III)-hydroxide Unit with Phenols

Debanjan Dhar[†≠], Gereon M. Yee[†≠], Todd F. Markle[‡], James M. Mayer*[‡] and William B. Tolman*[†]

[†]*Department of Chemistry, Center for Metals in Biocatalysis, University of Minnesota, 207 Pleasant St. SE, Minneapolis, MN 55455.* [‡]*Department of Chemistry, Yale University, New Haven, Connecticut 06520-8107*

[≠]These authors made equal contributions to this work. *Corresponding authors; *E-mail: james.mayer@yale.edu, wtolman@umn.edu*

Table of Contents

Experimental Details

Materials and Methods. All reagents and solvents were purchased from commercial sources and used as received unless otherwise noted. Tetrahydrofuran (THF) was either dried over sodium/benzophenone and vacuum distilled, or passed through activated alumina columns and plumbed directly into glove-box for direct use. Acetonitrile was dried over calcium hydride and vacuum distilled. Diethyl ether was passed through solvent purification columns (Glass Contour, Laguna, California). All solvents were stored over 3 Å molecular sieves in a N_2 filled glove-box prior to use. Metal complexes were synthesized and manipulated in a Vacuum Atmospheres glove-box under an inert atmosphere of N_2 or through use of standard Schlenk-line techniques. HPLC grade water was degassed by sparging with N_2 for 15 min prior to use in titration experiments. Elemental analyses were performed by Robertson Microlit Laboratory (Ledgewood, NJ). UV-vis spectra were obtained using an HP8453 (190-1100) diode array spectrophotometer. Variable temperature UV-vis experiments were performed using a Unisoku low temperature cell holder. Double mixing stopped flow UV-Vis absorption spectroscopy experiments were carried out on a TgK Scientific Double mixing Cryo Stopped-Flow instrument using a Xenon light source and a Kineta Scan Photodiode Array detector. X-ray diffraction measurements were collected with Cu Kα radiation and a Bruker D8 Photon II CPAD diffractometer using normal parabolic mirrors as monochromators. All GC-MS experiments were conducted on an Agilent Technologies 7890A GC system and 5975C VL MSD. The GC column was a HP-5 ms with dimensions 30 m x 0.25 mm. EPR spectra were recorded on a CW X-band Elexsys E500 EPR spectrometer equipped with an Oxford ESR 910 liquid helium cryostat. All spectra were recorded at a temperature of 30 or 77 K and at a microwave frequency of 9.64 GHz under the following conditions: microwave power of 0.063 mW (30 K) or 0.0002 mW (77 K); modulation amplitude of 9.8 G; modulation frequency of 100 kHz. Chemical shifts (δ) for ^{1}H and ^{13}C NMR spectra were referenced to residual protium in the deuterated solvent (^{1}H) or the characteristic solvent resonances of the solvent nuclei (^{13}C).

Compounds **1a**,[1] **1b**,[2] [Fc][BAr^F_4],[3] [AcFc][BAr^F_4],[2] (*p*-tolyl)$_3$NPF_6,[4] [$C_{12}H_8S_2$]PF_6,[5] and *p*-dimethylaminophenol[6] were synthesized as described previously.

[Bu_4N][^{NO2}ArO]. *4*-$NO_2C_6H_4OH$ (0.695 g, 5.00 mmol) was dissolved in anhydrous Et_2O (5 ml) and to this a solution of Bu_4NOH in MeOH (1.0 M, 5.0 ml, 5.0 mmol) was added. The yellow solution was stirred at room temperature for 30 min, after which the solvents were removed *in vacuo*. The resulting bright yellow solid was then suspended in anhydrous Et_2O (20 mL) and further stirred for 30 min, after which the residue was isolated by filtration and washed with excess Et_2O and dried thoroughly (1.62 g, 85.0%). ^{1}H NMR (DMSO-d_6, 400 MHz): δ_H 7.70 (2H, d), 5.87(2H, d), 3.14-3.18(8H, m), 1.49-1.61 (8H, m), 1.31 (8H, m), 0.93 (12H, t) ppm. $^{13}C\{^1H\}$ NMR (DMSO-d_6, 100 MHz): δ_C 127.51, 119.37, 57.51, 23.05, 19.20, 13.48 ppm.

[Bu_4N][LCu(^{NO2}ArO)]. LCu(MeCN)[1] (0.150 g, 0.255 mmol) and [Bu_4N][^{NO2}ArO] (0.098 g, 0.255 mmol) were suspended in anhydrous Et_2O (15 ml) and stirred for 30 min. After this, anhydrous THF (3 ml) was added to the suspension to facilitate dissolution of all solids and the resulting solution was allowed to stir at room temperature for 12 h. During the course of the reaction an olive green solid precipitated out of the reaction mixture. This solid was isolated by filtration and washed with copious amounts of anhydrous Et_2O and dried thoroughly (0.210 g, 88.7 %). X-ray quality crystals were obtained as green blocks by vapor diffusion of Et_2O into a concentrated solution of the compound in THF. UV-vis (THF, -80 °C) λ_{max}, nm (ε, M^{-1} cm^{-1}): 412 (23,100), 648 (800). Anal. Calcd for $C_{53}H_{77}CuN_5O_5.Et_2O$: C, 68.33; H, 8.75; N, 6.99. Found: C, 68.38; H, 8.66; N, 6.91.

Synthesis of 2,4,6-trimethylpyridinium Triflate. Dry HCl (g) (generated by dropwise addition of concentrated H_2SO_4 to NaCl) was passed over a stirring solution of 2,4,6-trimethylpyridine in Et_2O, yielding the 2,4,6-trimethylpyridinium hydrochloride salt as a white powder which was isolated by vacuum filtration, washed with Et_2O, and dried *in vacuo*. After taking this solid into a N_2 filled glovebox, the hydrochloride salt (0.250 g, 1.59 mmol) and AgOTf (0.450 g, 1.75 mmol) were transferred to a 20 mL vial and dissolved in dry acetonitrile (10 mL), resulting in the immediate formation of a white precipitate (AgCl). After stirring for

approximately 45 min, the suspension was passed through a syringe filter to remove AgCl, and the solvents were removed *in vacuo* to give a white oily solid. Trituration with 10-15 mL of dry Et_2O was followed by removal of the solvents *in vacuo*, and this was repeated three times, ultimately giving a white solid that was dried thoroughly *in vacuo* (0.350 g, 81.1%). ^{1}H NMR (DMSO-d_6, 400 MHz): δ_H 14.88 (1H, s), 7.58 (2H, s), 2.63 (6H, s), 2.49 (3H, s) ppm. $^{13}C\{^1H\}$ NMR (DMSO-d_6, 100 MHz): δ_C 159.07, 152.35, 125.52, 21.80, 19.43 ppm.

General procedure for double mixing stopped-flow monitoring of the reaction between $L_1Cu^{III}OH$ and 4-substituted phenols. In a N_2 filled glovebox, 0.12 mM stock solutions of **1a** and [Fc][$BAr^F{}_4$] in THF were prepared, along with stock solutions of the phenols, which ranged from 0.3-6 mM (5-100 eq.). Solutions were transferred to gas tight syringes fitted with luer-lock tips and transferred to the stopped flow syringes after thorough washing of the syringes and mixing lines with degassed THF (2.5 mL). A typical run involved initial 1:1 mixing of 0.12 mM solutions of **1a** and [Fc][$BAr^F{}_4$], yielding a reaction mixture which was aged for 4 s (to ensure full conversion of **1a** to **2a** as confirmed by single mixing experiments between **1a** and [Fc][$BAr^F{}_4$]). This was followed by a second 1:1 mixing event between the oxidized mixture and substrate solution, resulting in a final concentration of copper and substrate of 0.03 mM and 0.15-3 mM, respectively. Each mixing event resulted in a half-fold dilution of the starting solutions, and thus stock solutions of **1a** and [Fc][$BAr^F{}_4$] were prepared at four times the final concentration, whereas substrate stocks were prepared at twice the final concentration. After the final mixing event, UV-Vis snapshots were collected over the course of the reaction using an integration time of 0.002 s (except in the case of reactions involving 4-$Me_2NC_6H_4OH$ and 4-$MeOC_6H_4OH$, where an integration time of 0.0015 s was used).

Given that **2a** exhibits a characteristic charge transfer (CT) band at 548 nm (10,000 M^{-1} cm^{-1}), monitoring of the absorbance of this feature over time provided a nice handle by which to determine the rates for these reactions. In all cases, plots of absorbance vs. time fit well to a single exponential decay function (equation S1), yielding pseudo first-order rate constants (k_{obs}). Plots of k_{obs} vs. substrate concentration revealed a linear dependence, indicative of second-order

kinetics (for each kinetic step), and the slopes of these plots were taken as the second order rate constant (*k*, see equation S2).

$$[\mathrm{LCu^{III}OH}]_t = [\mathrm{LCu^{III}OH}]_0 e^{-k_{obs}t} \quad \text{(S1)}$$

$$k_{obs} = k_{self-decay} + k[\mathrm{Substrate}]_0 \quad \text{(S2)}$$

In addition to the method described above, global-fitting was also performed using the program Olis Global Works™.[7] In all cases, the rate constants provided from these fits are analogous to k_{obs} described above, and plotting these values against substrate concentration yielded very similar second-order rate constants when compared to those obtained from the single-wavelength analysis. All of the rate constants obtained from the pseudo first-order runs are summarized below in Table S1.

General procedure for double mixing stopped-flow monitoring of the stoichiometric reactions of 2a and b with 4-substituted phenols. In a N_2 filled glove box, 0.12 mM stock solutions of **1a**, **1b**, [Fc][BAr^F_4], and [AcFc][BAr^F_4] were prepared in THF, along with 0.06 mM stock solutions of the phenols. Solutions were transferred to gas tight syringes fitted with luer-lock tips and transferred to the stopped flow syringes after thorough washing of the syringes and mixing lines with degassed THF (2.5 mL). A typical run involved initial 1:1 mixing of 0.12 mM solutions of **1a**/**1b** and [Fc][BAr^F_4]/ [AcFc][BAr^F_4], yielding a reaction mixture which was aged for a set time (to ensure full conversion of **1a**/**1b** to **2a**/**2b** as confirmed by single mixing experiments between **1a**/**1b** and [Fc][BAr^F_4]/[AcFc][BAr^F_4]). This was followed by a second 1:1 mixing event between the oxidized mixture and substrate solution, resulting in a final concentration of 0.03 mM in both copper and substrate. Each mixing event resulted in a half-fold dilution of the starting solutions, and thus stock solutions of **1a**/**1b** and [Fc][BAr^F_4]/[AcFc][BAr^F_4] were prepared at four times the final concentration (0.12 mM), whereas substrate stocks were prepared at twice the final concentration (0.06 mM). After the

final mixing event, UV-vis snapshots were collected over the course of the reaction using an integration time of 0.002 s (except in the case of reactions involving 4-$Me_2NC_6H_4OH$ and 4-$MeOC_6H_4OH$, where an integration time of 0.0015 s was used). The absorbance of the charge transfer feature associated with either **2a**/**2b** (λ_{max}(ε, M^{-1} cm^{-1})= 548(10,000) or 500(13,300) nm for **2a**/**2b**, respectively) was monitored over time, and the decay absorbance trace was converted to concentration using the Beer-Lambert equation.[8] The initial 5-10% of the data was fit to a linear regression providing reaction rates (M/s) that were divided by the square of the $LCu^{III}OH$ concentration to give the second-order rate constant *k* (equation S3).[9]

$$-\frac{d[\mathrm{LCu^{III}OH}]}{dt} = k[\mathrm{LCu^{III}OH}][\mathrm{Substrate}] = k[\mathrm{LCu^{III}OH}]^2 \qquad \text{(S3)}$$

Comparison of the second-order rate constants obtained from the stoichiometric reactions with those from the pseudo-first order analysis reveals some clear discrepancies, specifically with regard to reactions with 4-NO_2- and 4-CF_3-phenol. These reactions are the slowest and include some significant contribution from self-decay in THF (discussed in detail previously).[2,10] In order to account for this, the data for these two runs were also fit to a mixed first and second order rate law to include a first order self-decay component (equation S4). Under conditions for which $[LCu^{III}OH]_0$ = $[Substrate]_0$, this can be approximated by equation S5, for with the integrated rate law is given by equation S6.[9] Using this analysis, second-order rate constants were obtained that agreed much more closely with those obtained from the pseudo first-order experiments.[11] Additionally, the rate constant obtained for self-decay from the fit is in good agreement with the independent self-decay rate measurements.[2,10]

$$-\frac{d[\mathrm{LCu^{III}OH}]}{dt} = k_1[\mathrm{LCu^{III}OH}] + k_2[\mathrm{LCu^{III}OH}][\mathrm{Substrate}] \qquad \text{(S4)}$$

When $[LCu^{III}OH]_0 = [Substrate]_0$, we can approximate $k_2[LCu^{III}OH][Substrate] = k_2[LCu^{III}OH]^2$. Thus the chemical equations for the first and second order steps are given below, along with their corresponding rate equations

$$LCu^{III}OH \rightarrow X, \text{rate}_1 = k_1[LCu^{III}OH]$$

$$LCu^{III}OH + LCu^{III}OH \rightarrow Y, \text{rate}_2 = k_2[LCu^{III}OH]^2$$

Given that the second step involves the reaction of 2 molecules of $LCu^{III}OH$, $-d[LCu^{III}OH]/dt$ for the second step is 2x rate_2. Thus the overall rate of change of $[LCu^{III}OH]$ can be written as

$$-\frac{d[LCu^{III}OH]}{dt} = rate_1 + 2rate_2 = k_1[LCu^{III}OH] + 2k_2[LCu^{III}OH]^2 \qquad \text{(S5)}$$

For which the integrated rate law is given as

$$[LCu^{III}OH]_t = \frac{k_1[LCu^{III}OH]_0 e^{-k_1 t}}{k_1 + 2k_2[LCu^{III}OH]_0(1 - e^{-k_1 t})} \qquad \text{(S6)}$$

It is important to note that while the stoichiometric data for reactions of **2a/b** with ^{NO2}ArOH and ^{CF3}ArOH indeed fit better to equation S6, we have assumed in applying the rate equation S5 that over the course of the reaction, $[LCu^{III}OH]_t = [Substrate]_t$. While we acknowledge that this is not actually the case, we posit that $[LCu^{III}OH]_t$ and $[Substrate]_t$ do not diverge significantly over the course of the reaction; the change in $[LCu^{III}OH]_t$ due to self-decay, though significant, is still relatively small.

For the faster reactions, fits to equation S6 were of lower quality and gave physically unreasonable values, a reflection of the diminishing contribution of self-decay to the overall rate. Thus, this correction was only applied to reactions with the 4-NO_2- and 4-CF_3-phenols. The second-order rate constants for the stoichiometric reactions of **2a**/**2b** with phenolic substrates are summarized below in Table S2.

Identification of Radical Species in reactions of 2a 2,4,6-tri-t-butylphenol and TEMPOH. A dry 2 mm EPR tube was capped with a rubber septum and cooled in a liquid N_2/acetone bath under active Ar flow. The tube was charged with [Fc][BAr^F_4] (0.3 mL at 1.67 mM concentration) via syringe and allowed to cool for approximately 5-10 min. A solution of **1a** (0.1 mL, 5 mM in THF) was subsequently added, giving a deep purple solution, which was mixed by slow sparging with Ar gas. To this mixture was added 0.1 mL of substrate (10 mM TEMPOH or 2,4,6-tri-*t*-butylphenol in THF), and the solution was sparged with Ar gas for approximately 15-20 min at -80 ºC, after which the solution was frozen in liquid N_2 under active Ar flow. These samples were then analyzed by EPR spectroscopy to identify the presence of organic radical species in solution (conditions: 1 mM final concentration, 77 K, 0.0002 mW microwave power; see Figure S8 below).

Identification of Radical Species in UV-vis reactions of 2b with 2,4,6-tri-t-butylphenol. In a N_2 filled glove-box, a 3 mL cuvette was charged with 1.8 mL of dry THF and 0.1 mL of a 2 mM solution of **1b**. The cuvette was capped with a rubber septum, taken out of the glove-box, and cooled in the spectrometer at -80 ºC for 10 minutes under a slow Ar flow. To the cooled solution was added [AcFc][BAr^F_4] (0.1 mL, 2 mM), which resulted in the growth of a charge transfer feature at 513 nm, characteristic of **2b**. To this solution was added 0.1 mL of 2 mM 2,4,6-tri-*t*-butylphenol, which resulted in the rapid decay of this feature. Once this feature had completely decayed, an aliquot of this solution was transferred to a 2 mm EPR tube and analyzed by EPR spectroscopy for the presence of organic radical products in solution (conditions: 0.1 mM concentration, 30 K, 0.063 mW microwave power; see Figure S8 below).

EPR Identification of Fc^+ in the product solutions of reactions between 2a and ^{NO2}ArOH. A dry 2 mm EPR tube was capped with a rubber septum and cooled in a liquid N_2/acetone bath (~ -80 ºC) under active N_2 flow. The tube was charged with [Fc][BAr^F_4] (0.1 mL, 3 mM in THF) via syringe and allowed to cool for approximately 5-10 min. A solution of **1a** (0.1 mL, 3 mM in THF) was subsequently added, giving a deep purple solution, which was mixed by slow sparging with N_2 gas. To this mixture was added 0.1 mL of substrate (3 mM

^{NO2}ArOH), and the solution was slowly sparged with N_2 gas for approximately 15-20 min at -80 ºC, after which the solution was frozen in liquid N_2 under active N_2 flow. These samples were then analyzed by EPR spectroscopy to identify the presence of Fc^+ in solution (conditions: 1 mM concentration, 30 K, 2 mW microwave power; see Figure S22 below). For comparison, a 1 mM sample of $FcBAr^F_4$ in THF was prepared and recorded under the same conditions (see Figure S22 below).

UV-Vis Quantification of 2,4,6-tri-t-butylphenoxyl Radical in Reactions of 2a with 2,4,6-tri-t-butylphenol. In a N_2 filled glovebox, a 3 mL cuvette was charged with 1.8 mL of THF. The cuvette was capped with a rubber septum, taken out of the glovebox, and cooled in the spectrometer at -80 ºC under a slow Ar flow. To this was added 0.1 mL of a 2 mM solution of **1a** in THF, followed by 0.1 mL of a 2 mM solution of $[AcFc][BAr^F_4]$, which resulted in the immediate growth of a charge transfer band centered at 548 nm, characteristic of **2a**. Subsequent addition of 0.1 mL of 4 mM 2,4,6-tri-*t*-butylphenol resulted in the decay of this feature and the appearance of sharp charge transfer features centered near 400 nm, indicative of the formation of 2,4,6-tri-*t*-butylphenoxyl radical. This species was quantified using the measured absorbance and the known molar extinction coefficient.[12]

General procedure for analysis of products from reactions of 2a and 2b with substituted phenols (3a-g). This procedure is adapted from previously reported procedure. In a N_2 filled glovebox, 5.4 mL of a THF solution of **1a** or **1b** (5.56 mM) and a magnetic stir bar were transferred to a 20 mL vial that was capped with a rubber septum secured with copper wire. This was taken out of the glovebox and cooled to -80 ºC in an acetone/liquid N_2 bath under a slow, active flow of N_2, supplied through a needle via the Schlenk line. After cooling for approximately 10 min, 0.3 mL of a THF solution of $[Fc][BAr^F_4]$ or $[AcFc][BAr^F_4]$ (100 mM) was quickly added with stirring, resulting in a deep purple colored solution. After waiting approximately 30 s, a THF solution of *p*-cresol was quickly added (0.3 mL @ 200 mM), resulting in a rapid color change to a more brown/green color. This solution was allowed to stir for an additional 30 min at low temperature before $HClO_4$ (0.2 mL @ 4 M) was added to quench

the reaction, followed by warming of the solution to room temperature. After adding 2-5 mL of H_2O, THF was removed by rotary evaporation, after which the remaining aqueous mixture was extracted with ethyl acetate (3 x 10 mL). The combined organic phases were washed with brine (2 x 10 mL), dried over Na_2SO_4 and filtered, and finally concentrated to dryness by rotary evaporation, generally giving an oily/solid residue. To the product mixture was added 2 mL of acetone, 1 mL of which was filtered through a 0.2 μm syringe filter into a GC-MS vial that was spiked with 0.05 mL of 25 mM 1,3,5-trimethoxybenzene in acetone as an internal standard.

Final quantification was then performed using GC-MS to measure the percentage of product in the sample relative to internal standard, which was measured against a calibration curve. This curve was prepared using a coupled phenol surrogate, namely 2,2'-biphenol, given its ready availability and chemical similarity to the expected C-C coupled phenol products. The standard method used for all runs involved injection into an initial oven temperature of 50 °C (held for 2 min) followed by a 20 °C min^{-1} ramp to 70 °C (held for 6 min), followed by a 20 °C min^{-1} ramp to 150 °C (held for 3 min), followed by a final 20 °C min^{-1} ramp to 250°C (held for 8 min). The flow rate of He carrier gas was 1 mL/min and the inlet temperature was 250 °C.

General procedure for the generation of [LCu(OH$_2$)]$^+$ (4a) by oxidation. A 3 mL cuvette capped with a rubber septum was charged with anhydrous acetone (1.95 mL) and degassed HPLC grade water (0.05 mL) under Ar. The cuvette was cooled at -80 ºC for 10 min, after which a solution of LCu(THF) in acetone (0.1 mL, 2 mM) was added. Subsequent addition of an MeCN solution of $[C_{12}H_8S_2]PF_6$ (0.1 mL, 2 mM) resulted in the immediate growth of an intense charge transfer feature centered at ~ 550 nm, for which the UV-vis spectrum was recorded.

General procedure for the generation of [LCu(OH$_2$)]$^+$ (4a) by protonation of LCuOH (2a). In an N_2 filled glove-box, a 3 mL cuvette was charged with THF (1.8 mL) and a THF solution of **1a** (0.1 mL, 1 mM), and capped with a rubber septum. The cuvette was then taken out of the glove-box and cooled at -80 ºC for 10 min, after which an MeCN solution of $[C_{12}H_8S_2]PF_6$ (0.1 mL, 1 mM) was added, resulting in the growth of an LMCT band at 548 nm characteristic of

2a. Subsequently, a THF solution of 2,4,6-trimethylpyridinium triflate (0.1 mL, 1 mM) was added and the UV-vis spectrum was recorded.

General procedure for the observation of intermediate 4a in reactions of LCuOH with ^{NO2}ArOH and ^{Me}ArOH. In an N_2 filled glove-box, a 3 mL cuvette was charged with THF (1.8 mL) and a THF solution of **1a** (0.1 mL, 1 mM), and capped with a rubber septum. The cuvette was then taken out of the glove-box and cooled at -80 ºC for 10 min, after which an MeCN solution of either $[(p\text{-tolyl})_3N]PF_6$ or $[C_{12}H_8S_2]PF_6$ (0.1 mL, 1 mM) was added, resulting in the growth of an LMCT band at 548 nm characteristic of **2a**. Subsequently, a THF solution of either ^{NO2}ArOH or ^{Me}ArOH (0.1 mL, 2 mM) was added and UV-vis spectra were monitored over time.

General procedure for the oxidation of LCu(THF) with $[C_{12}H_8S_2]PF_6$ in THF. In an N_2 filled glove-box, a 3 mL cuvette was charged with THF (1.8 mL) and a THF solution of LCu(THF) (0.1 mL, 2 mM), and capped with a rubber septum. The cuvette was then taken out of the glove-box and cooled at -80 ºC for 10 min, after which 0.05 mL aliquots of an MeCN solution of $[C_{12}H_8S_2]PF_6$ (0.1 mL, 1 mM) were added, resulting in the growth of multiple intense charge transfer features centered at ~ 534, 735, and 992 nm. The resulting UV-vis spectrum was recorded.

General procedure for the oxidation of $[Bu_4N][LCuOAr^{NO2}]$ with $[(p\text{-tolyl})_3N]PF_6$ in THF. In an N_2 filled glove-box, a 3 mL cuvette was charged with THF (2.4 mL) and a THF solution of $[Bu_4N][LCuOAr^{NO2}]$ (0.1 mL, 1 mM), and capped with a rubber septum. The cuvette was then taken out of the glove-box and cooled at -80 ºC for 10 min, after which an MeCN solution of $[(p\text{-tolyl})_3N]PF_6$ (0.1 mL, 1 mM) was added, resulting in the growth of two intense charge transfer features centered at ~ 656 and 814 nm. The resulting UV-vis spectrum was recorded.

Table S1. Second-order Rate Constants for Pseudo First-Order Reactions of **2a** with ^{X}ArOH.

X	**2a**^{a,b}	**2a**^{a,c}
NMe_2	-	-
OMe	$(3.0 \pm 0.5) \times 10^5$	$(2.7 \pm 0.4) \times 10^5$
Me	$(8.9 \pm 1.3) \times 10^3$	$(9.6 \pm 1.4) \times 10^3$

H	$(3.9 \pm 0.6) \times 10^2$	$(3.9 \pm 0.6) \times 10^2$
Cl	$(6.5 \pm 1.0) \times 10^2$	$(6.4 \pm 1.0) \times 10^2$
NO_2	$(2.6 \pm 0.4) \times 10^2$	$(2.1 \pm 0.3) \times 10^2$
NO_2	-	$(1.7 \pm 0.2) \times 10^{3d}$
CF_3	$(3.0 \pm 0.5) \times 10^1$	$(1.8 \pm 0.3) \times 10^1$
CF_3	-	$(8.4 \pm 1.3) \times 10^{2d}$

[a] *k* has units of M^{-1} s^{-1}; errors are reported either as the statistical error from the fits or as a flat 15%, whichever is larger. [b] Pseudo first-order analysis of single wavelength absorbance vs. time traces. [c] From global fits to pseudo first-order UV-vis spectra using Olis Global Works™ program. [d] Second rate constant obtained for the A→B→C model as determined from global fits.

Table S2. Second-order Rate Constants for Stoichiometric Reactions of **2a** and **2b** with ^{X}ArOH Determined from Initial Rates

X	**2a**[a]	**2b**[a]
NMe_2	$(1.9 \pm 0.3) \times 10^6$	$(6.7 \pm 1.0) \times 10^6$
OMe	$(3.0 \pm 0.5) \times 10^5$	$(1.8 \pm 0.3) \times 10^6$
Me	$(7.0 \pm 1.1) \times 10^3$	$(1.0 \pm 0.2) \times 10^6$
H	$(5.1 \pm 0.8) \times 10^2$	$(1.8 \pm 0.3) \times 10^5$
Cl	$(5.7 \pm 0.9) \times 10^2$	$(1.4 \pm 0.2) \times 10^5$
NO_2 [b]	$(1.9 \pm 0.3) \times 10^2$	$(8.2 \pm 2.6) \times 10^2$
NO_2	$(4.6 \pm 0.7) \times 10^2$	$(1.7 \pm 0.5) \times 10^3$
CF_3 [b]	$(3.0 \pm 0.5) \times 10^1$	$(3.0 \pm 1.5) \times 10^2$
CF_3	$(3.0 \pm 0.5) \times 10^2$	$(7.6 \pm 3.1) \times 10^2$

[a] *k* has units of M^{-1} s^{-1}; errors are reported either as the statistical error from the fits or as a flat 15%, whichever is larger. [b] Determined from fits to mixed first- and second-order equation (equation S6). Values of k_1 for reactions with **2a** and **2b** were found to be $(4.7 \pm 0.3) \times 10^{-3}$ s^{-1} and $(8.0 \pm 0.4) \times 10^{-3}$ s^{-1}, respectively.

Table S3. Hydrogen bond donor activities of the phenols used in this study.

Phenol	*4-CF_3*	*4-NO_2*	*4-Cl*	*4-H*	*4-Me*	*4-OMe*	*4-NMe_2*
α [a]	0.724	0.787	0.670	0.596	0.569	0.573	0.57**

[a] Adapted from Ref 13. ** Determined from Hammett parameters as discussed in Ref 13c.

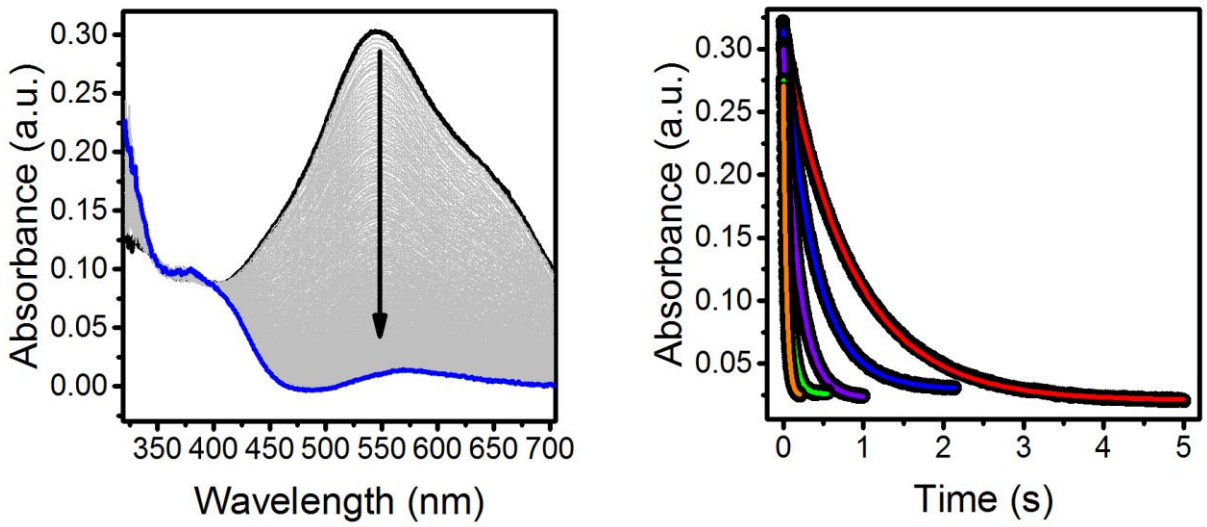

Figure S1. (Left) Representative pseudo first-order UV-vis decay trace of **2a** in the presence of a ^{Me}ArOH, as monitored by stopped-flow studies. The final blue spectrum matches that of the LCu(THF) adduct (see Figure S10 below), which forms as a result of ligand exchange with **3a**. (Right) Representative fits of the absorbance at 548 nm to a single exponential decay function.

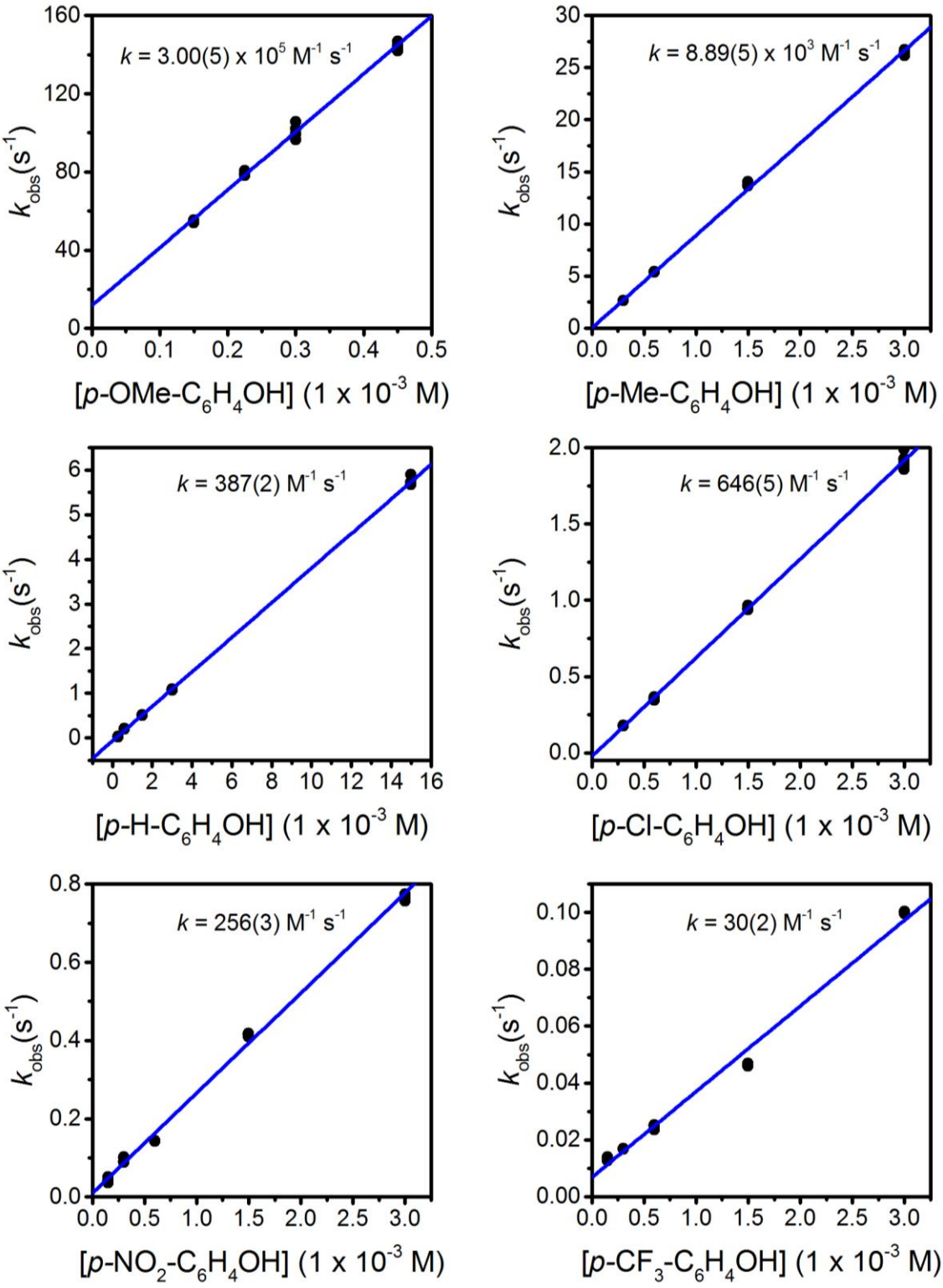

Figure S2. Second-order plots for pseudo-first order reactions of **2a** with *p*-OMe- (top left), *p*-Me- (top right), *p*-H- (middle left), *p*-Cl- (middle right), *p*-NO_2- (bottom left), and *p*-CF_3-phenol (bottom right). Pseudo first-order rate constants (k_{obs}) were determined using single wavelength analysis, exemplified in Figure S1 above.

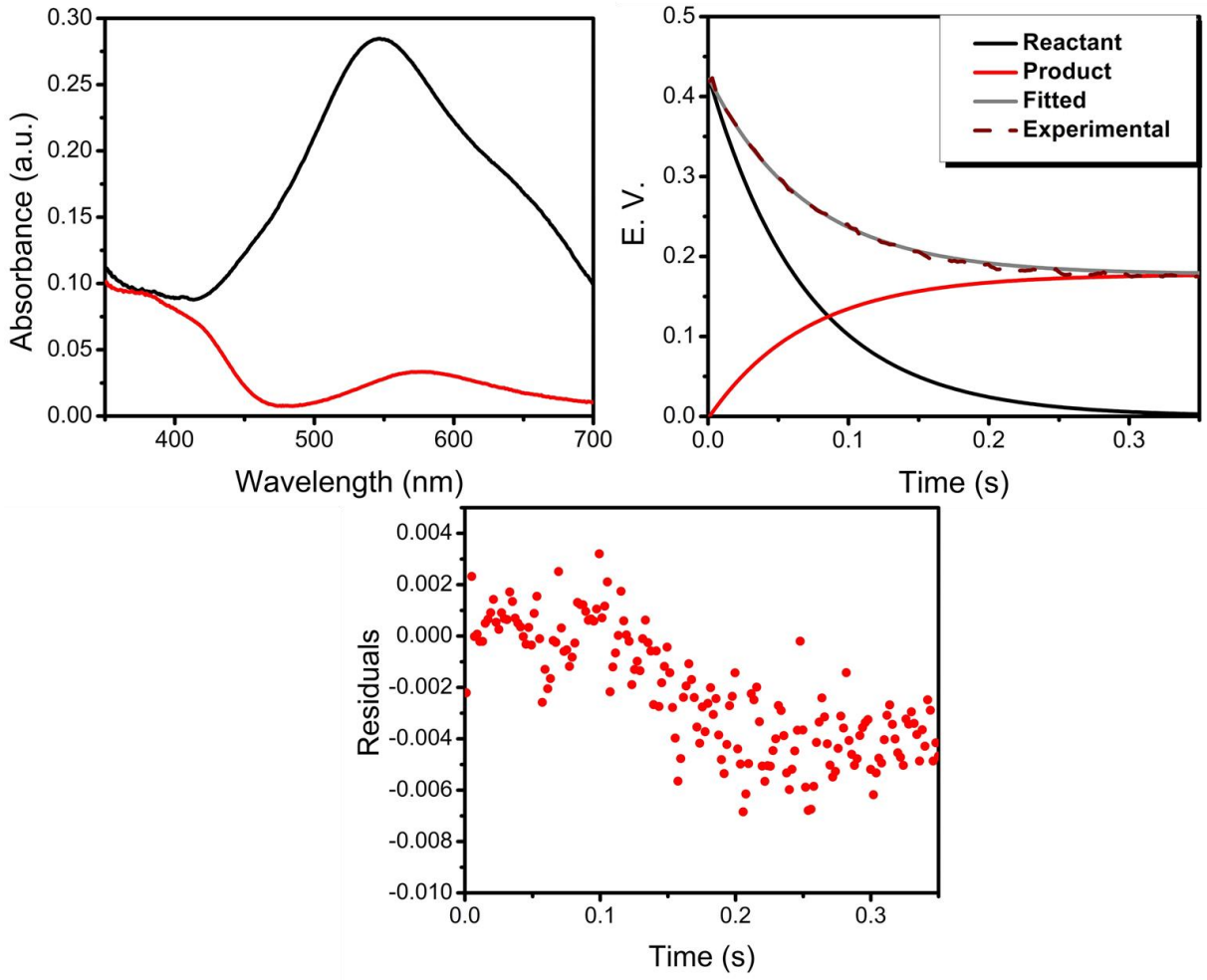

Figure S3. Representative spectral components obtained from the global kinetic analysis using Olis Global Works™ for *p*-cresol reacting with **2a** under pseudo-first order conditions in which reactant is in black and product is in red (top left). Relative contribution of the respective spectral components (or eigen vectors, E.V.) to the overall observed spectrum over the course of time; This represents the time course evolution of the various species involved in the reaction (top right). Plot of residuals (bottom).

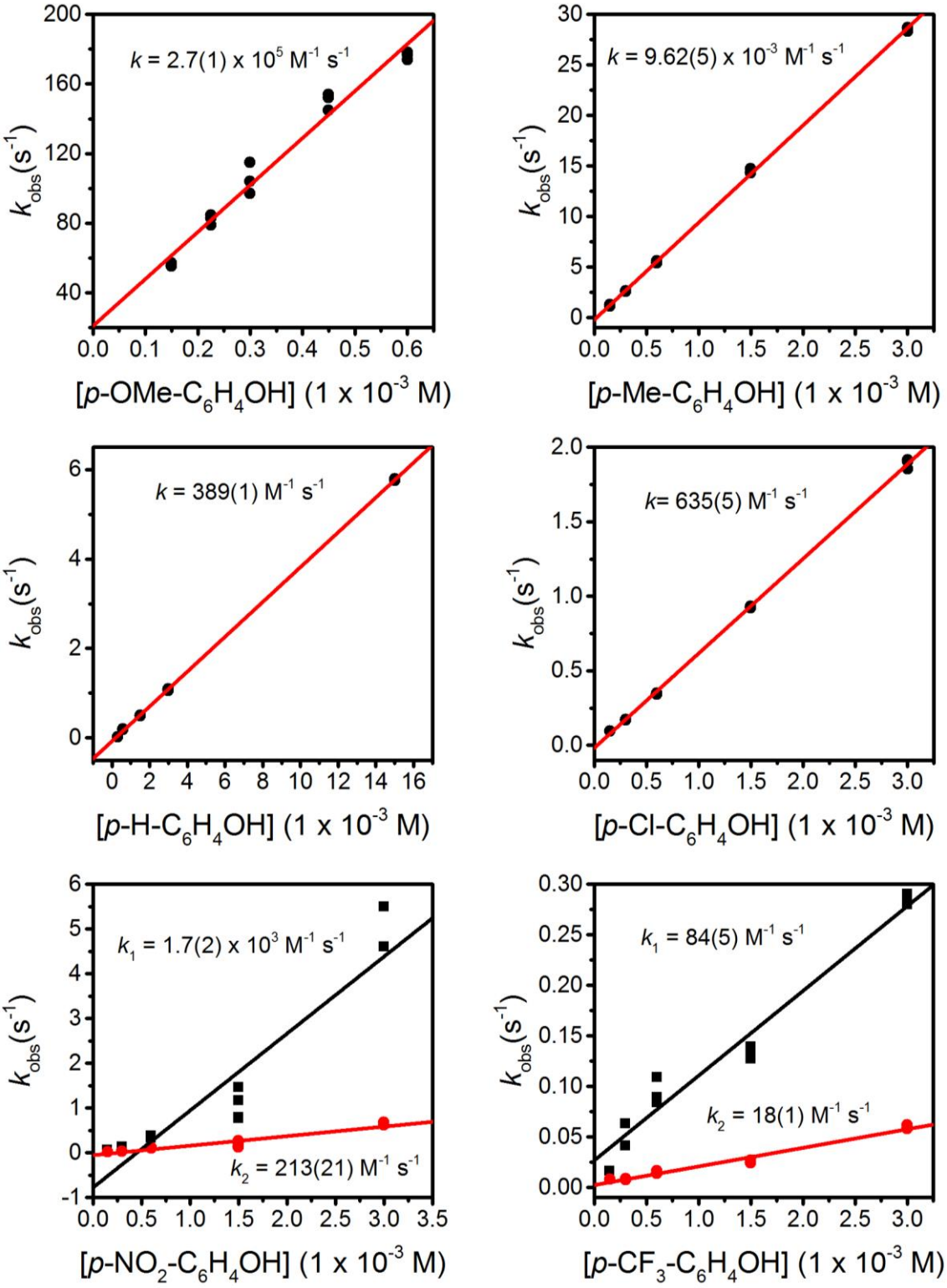

Figure S4. Second-order plots for pseudo-first order reactions of **2a** with *p*-OMe- (top left), *p*-Me- (top right), *p*-H- (middle left), *p*-Cl- (middle right), *p*-NO_2- (bottom left), and *p*-CF_3-phenol (bottom right). Pseudo first-order rate constants (k_{obs}) determined from global fitting with Olis Global Works™ program, exemplified in Figure S3 above.

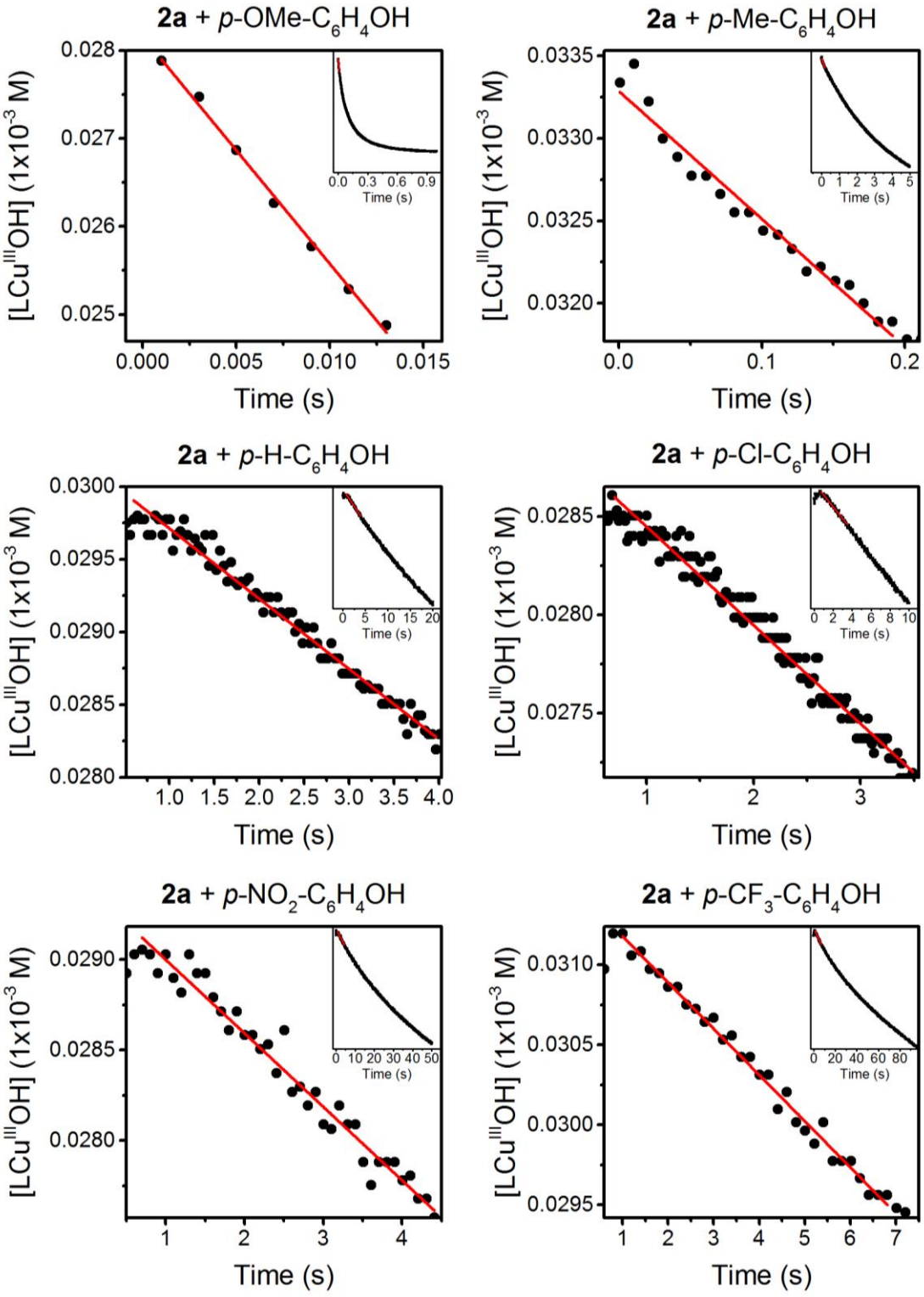

Figure S5. Plots of [LCu^{III}OH] vs. time (black) along with linear fits to the first 5% of data (10% in the case of *p*-OMe-phenol) for stoichiometric reactions of **2a** with *p*-OMe- (top left), *p*-Me- (top right), *p*-H- (middle left), *p*-Cl- (middle right), *p*-NO_2- (bottom left), and *p*-CF_3-phenol (bottom right).

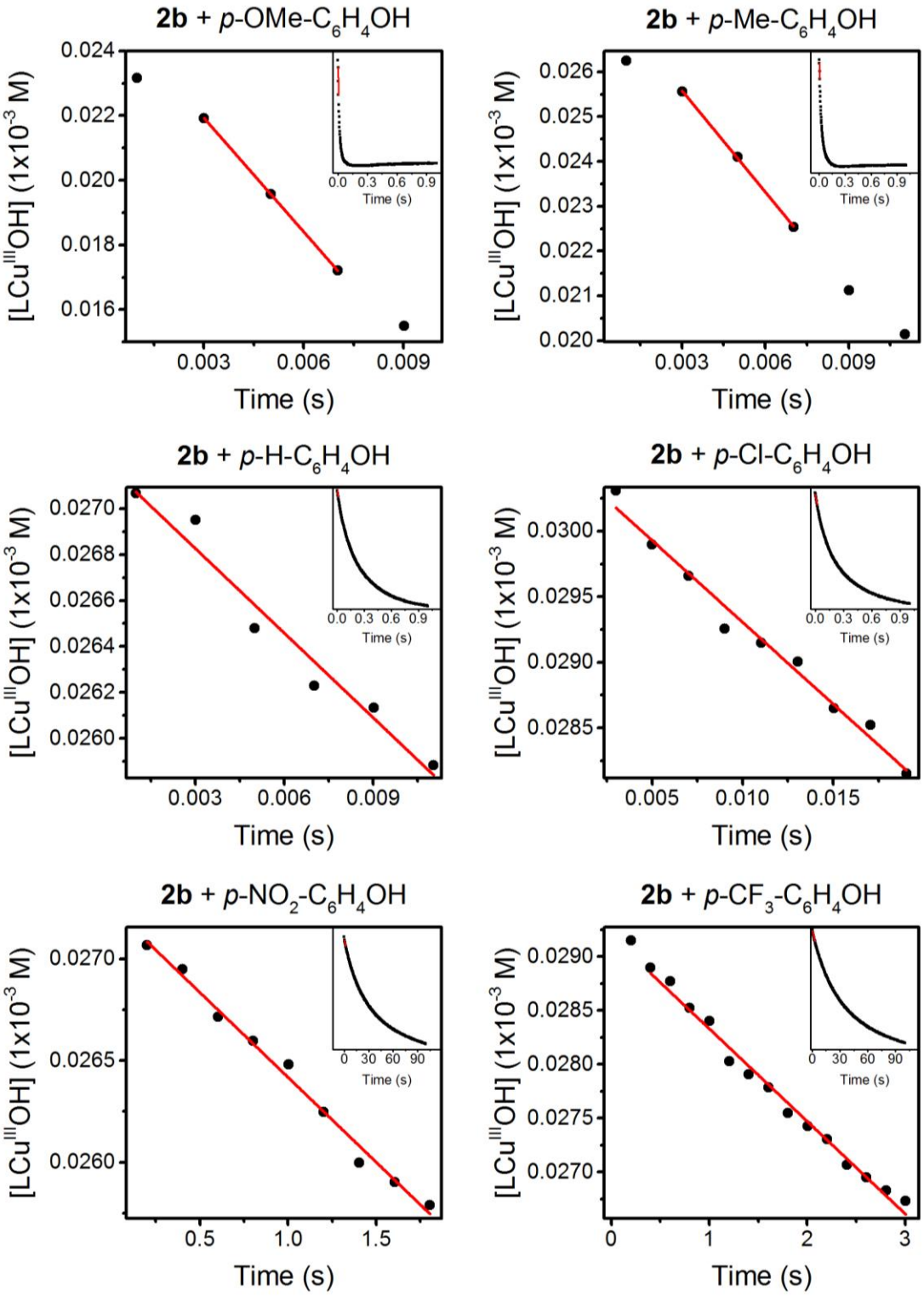

Figure S6. Plots of [LCu^{III}OH] vs. time (black) along with linear fits to the first 5% of data (10% in the case of *p*-OMe-phenol) for stoichiometric reactions of **2b** with *p*-OMe- (top left), *p*-Me- (top right), *p*-H- (middle left), *p*-Cl- (middle right), *p*-NO_2- (bottom left), and *p*-CF_3-phenol (bottom right).

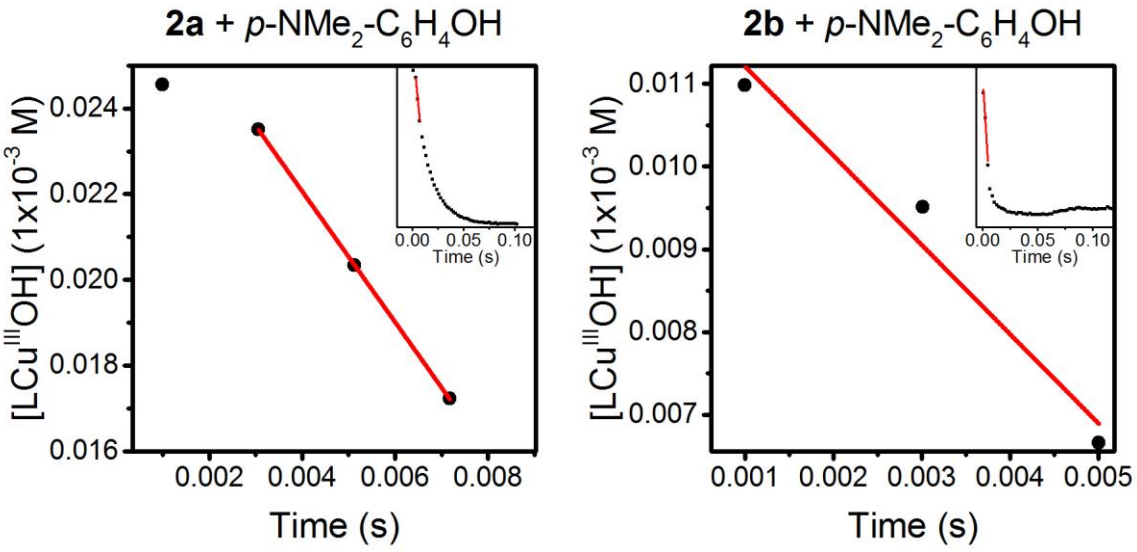

Figure S7. Plots of [LCu^{III}OH] vs. time (black) along with linear fits (red) to the first three-four data points for stoichiometric reactions of **2a** (left) and **2b** (right) with *p*-NMe$_2$-phenol.

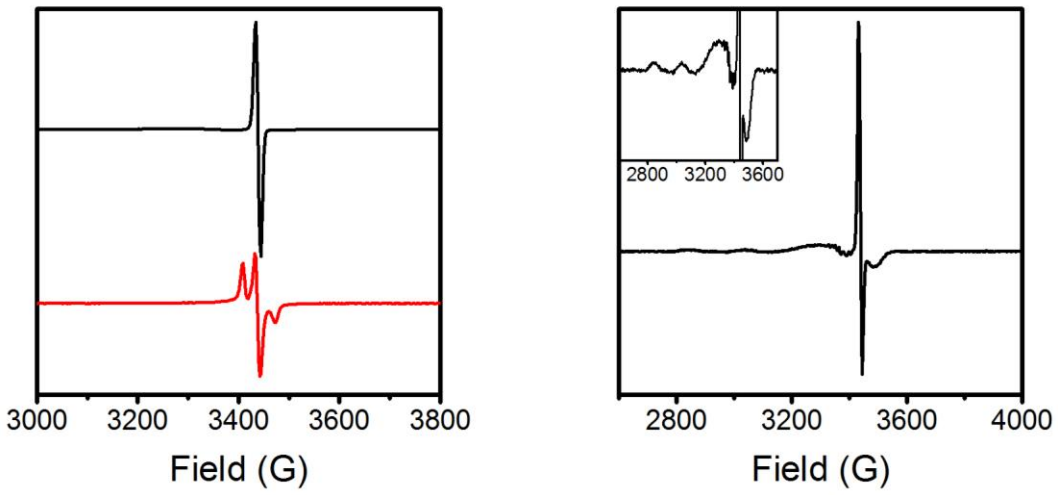

Figure S8. (Left) EPR spectra for reactions of **2a** with 2,4,6-tri-*t*-butylphenol (black) and TEMPOH (red), confirming the formation of organic radical species in these reactions (conditions: 1 mM concentration, 77 K, 0.0002 mW microwave power). (Right) Product EPR spectrum for reaction of **2b** with 2,4,6-tri-*t*-butylphenol confirming the formation of phenoxyl radical in this reaction (conditions: 0.1 mM concentation, 30 K, 0.063 mW microwave power). The inset shows a zoomed in view to highlight the copper features that are also observed.

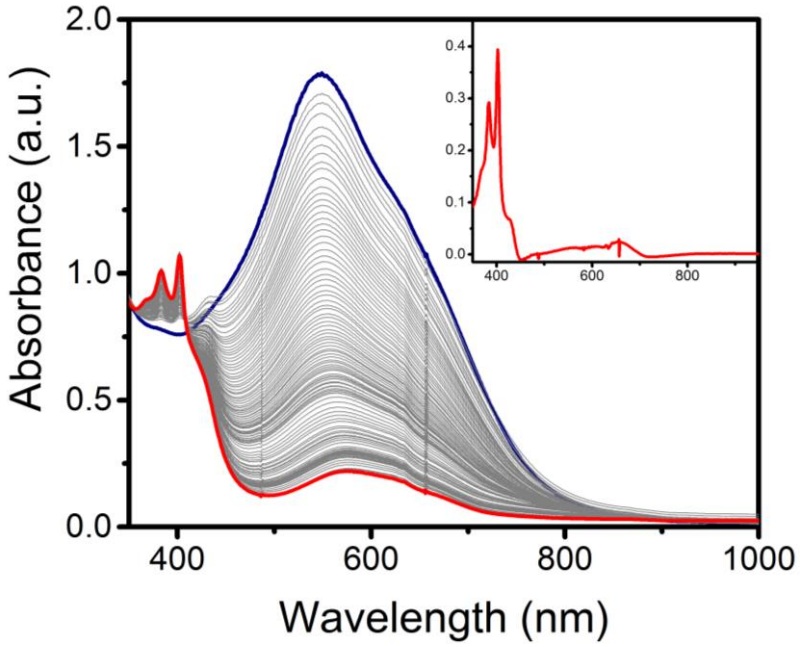

Figure S9. UV-vis traces of reaction between **2a** and 2 eq. 2,4,6-tri-*t*-butylphenol in THF monitored at -80 °C. The inset shows the spectrum of the phenoxyl radical obtained after subtracting out the spectral contribution from other species in solution.

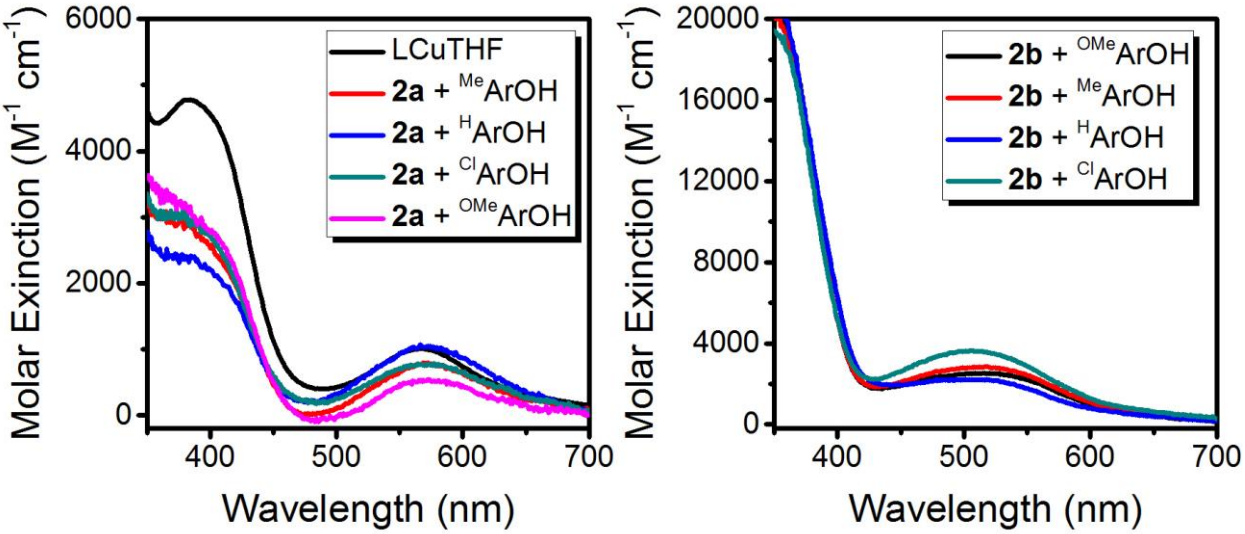

Figure S10. (Left) Final decay spectra of pseudo first-order stopped-flow reactions between **2a** and ^{Me}ArOH (red), ^{H}ArOH (blue), ^{Cl}ArOH (green), and ^{OMe}ArOH (pink), all overlayed with an independent spectrum of LCu(THF) (black), supporting the identity of this species as the final inorganic product from these reactions. (Right) Final decay spectra of stoichiometric stopped-flow reactions between **2b** and ^{OMe}ArOH (black), ^{Me}ArOH (red), ^{H}ArOH (blue), and ^{Cl}ArOH (green).

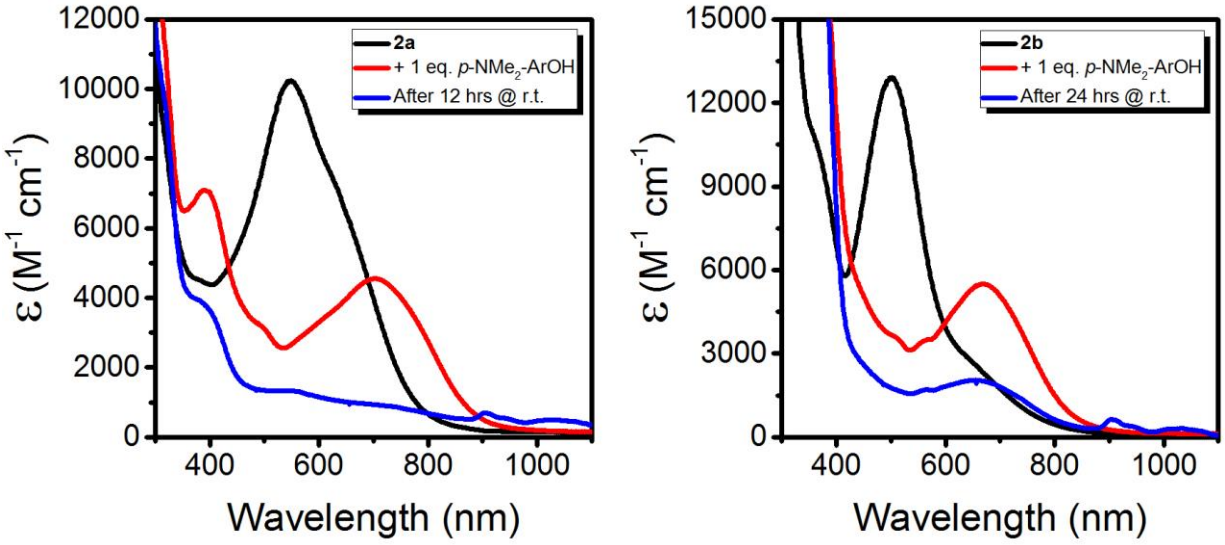

Figure S11. UV-vis traces showing the reaction between **2a** (left) or **2b** (right) with 1 eq. of ^{NMe2}ArOH and the corresponding decay spectra after prolonged warming at room temperature. The starting spectra of **2a/b** are shown in black, the resulting spectra after the addition of 1 eq. of ^{NMe2}ArOH are shown in red, and the decay spectra are shown in blue.

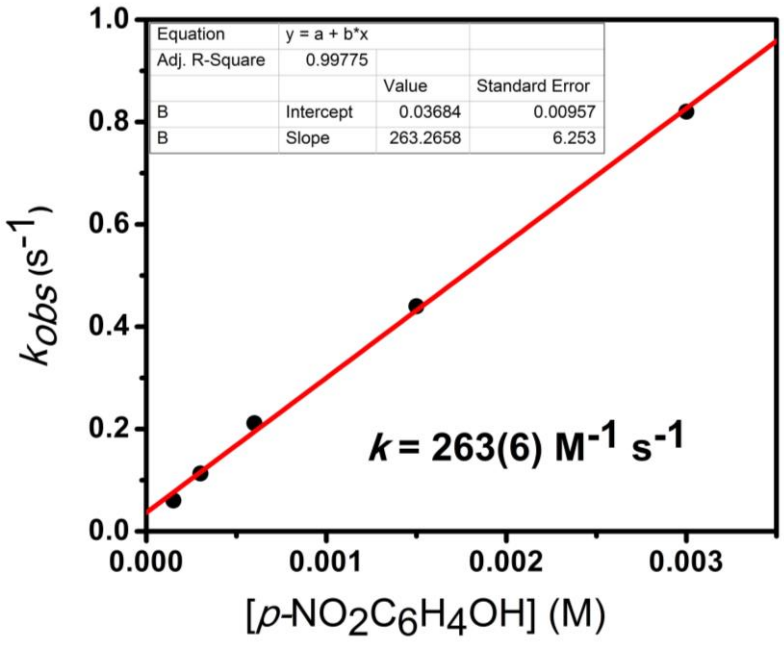

Figure S12. Second-order plots for pseudo-first order reactions of **2a** with *p*-NO_2-phenol. Pseudo first-order rate constants were determined using single wavelength analysis by fitting the growth of the charge transfer feature at 400 nm to a single exponential function.

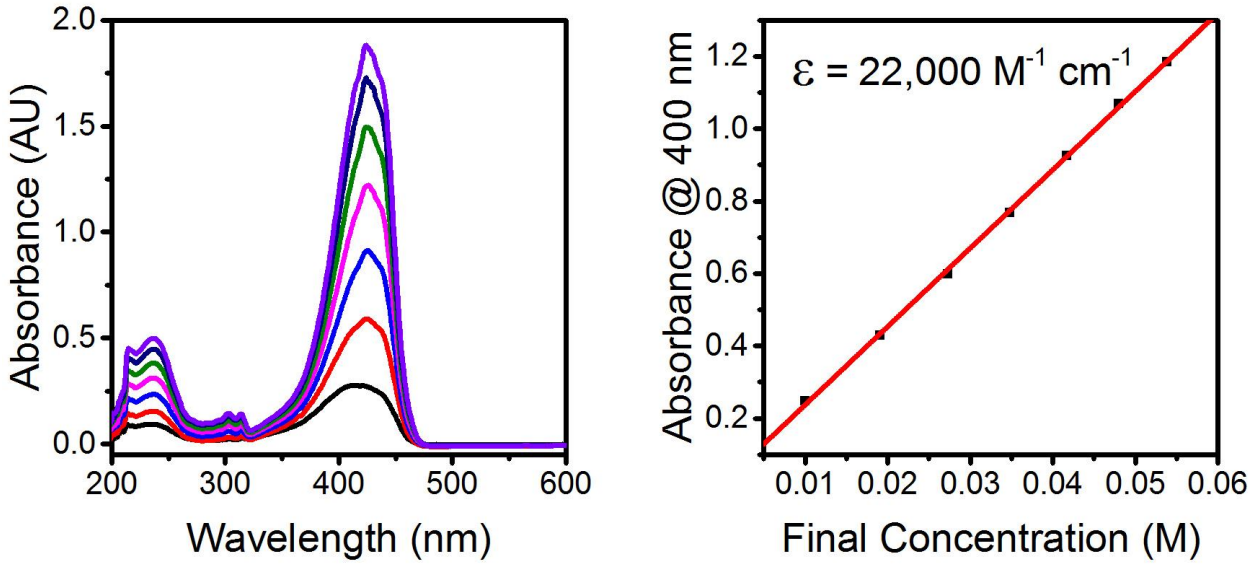

Figure S13. UV-vis spectra (left) and corresponding Beer's law plot (right) for the absorbance at 400 nm for $(Bu_4N)(^{NO2}ArO)$.

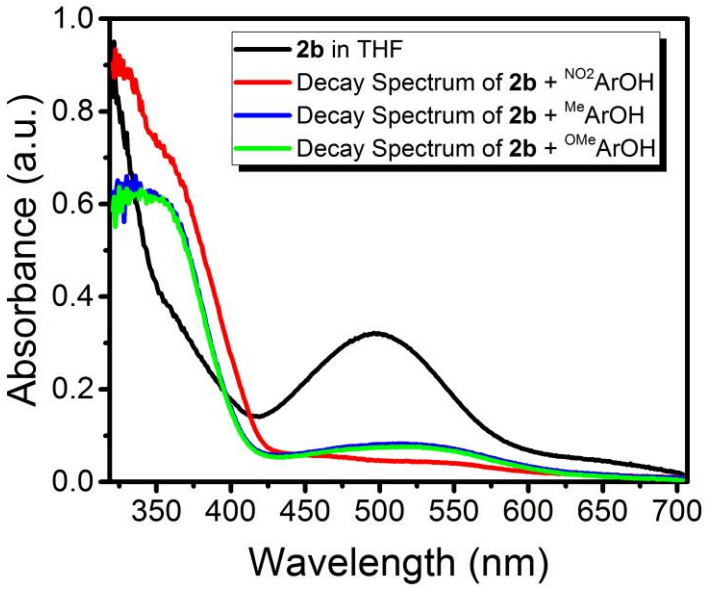

Figure S14. UV-Vis spectrum of **2b** in THF at -80 ºC (black) and ending spectra for reactions between **2b** and ^{NO2}ArOH (red), ^{Me}ArOH (blue), and ^{OMe}ArOH (green), highlighting the difference in the final absorbance at 400 nm for the reaction with ^{NO2}ArOH relative to the other two substrates.

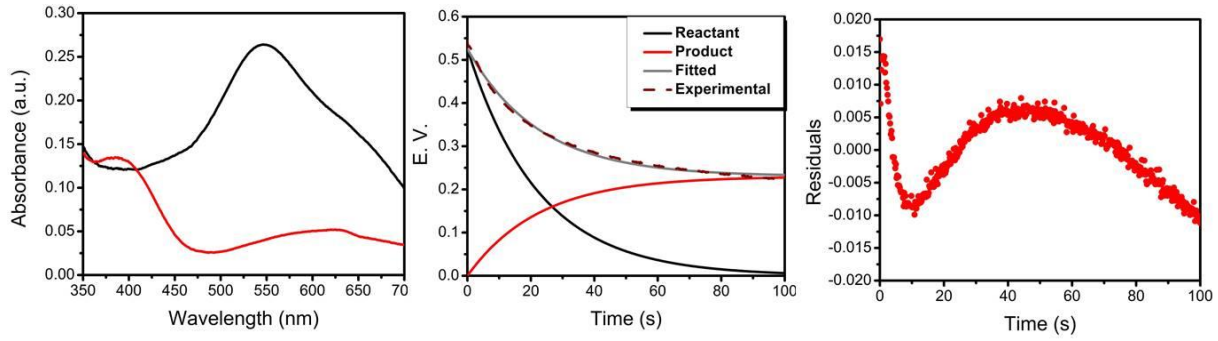

Figure S15. Representative spectral components obtained from the attempted global kinetic analysis using a simple kinetic model (A→ B) on Olis Global Works for *p*-CF_3-phenol reacting with **2a** under pseudo-first order conditions in which reactant is in black and product is in red (left). Relative contribution of the respective spectral components (or eigen vectors, E.V.) to the overall observed spectrum over the course of time; this represents the time course evolution of the various species involved in the reaction (center). Plot of residuals indicating a systematic error in the fits (right).

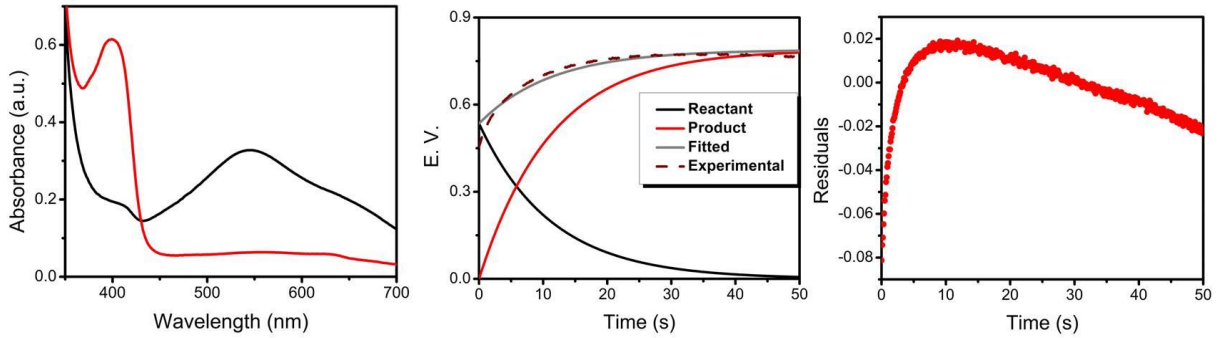

Figure S16. Representative spectral components obtained from the attempted global kinetic analysis using a simple kinetic model (A→ B) on Olis Global Works for *p*-NO_2-phenol reacting with **2a** under pseudo-first order conditions in which reactant is in black and product is in red (left). Relative contribution of the respective spectral components (or eigen vectors, E.V.) to the overall observed spectrum over the course of time; this represents the time course evolution of the various species involved in the reaction (center). Plot of residuals indicating a systematic error in the fits (right).

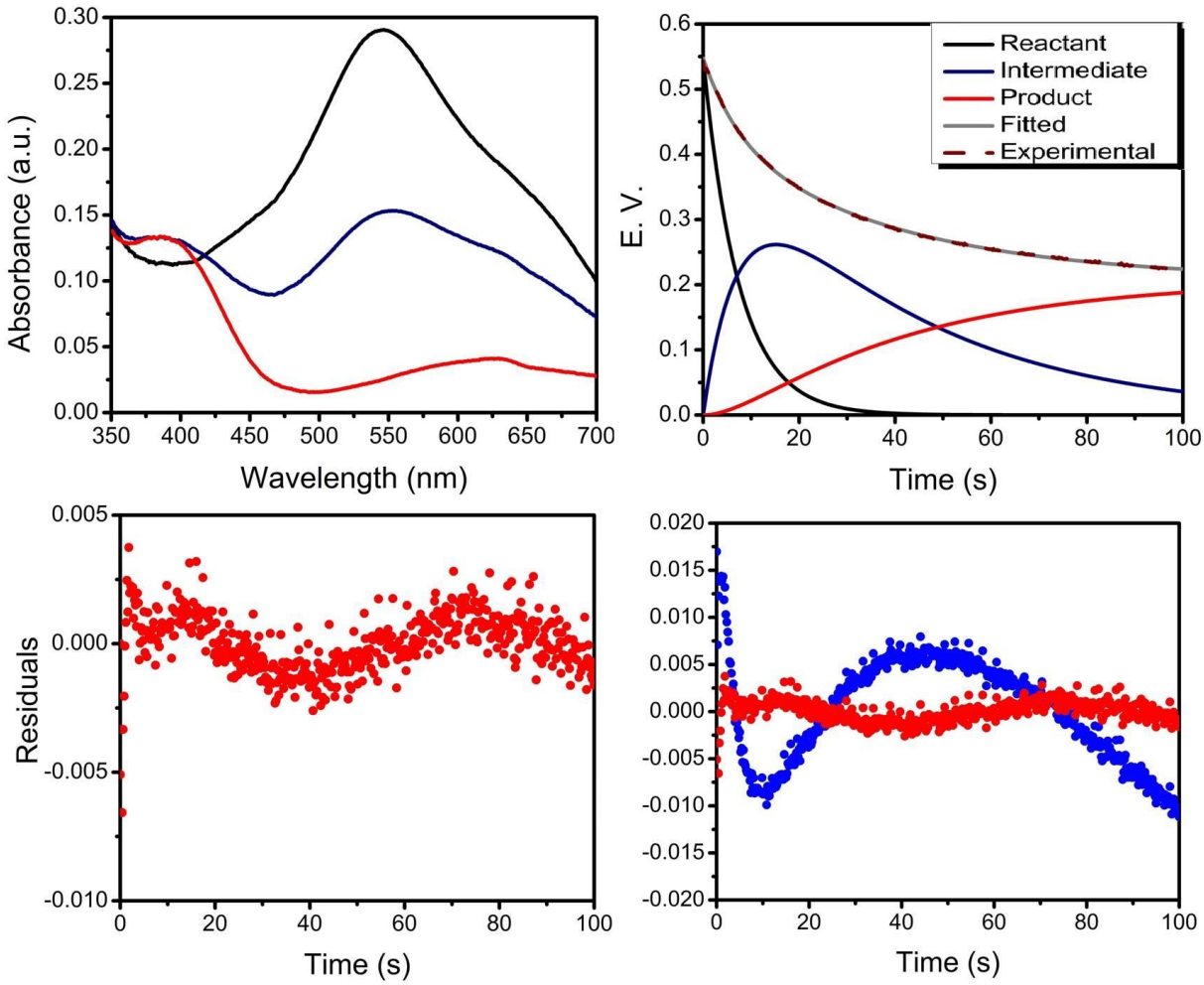

Figure S17. Representative spectral components obtained from the global kinetic analysis using Olis Global Works for *p*-CF_3-phenol reacting with **2a** under pseudo-first order conditions when the kinetic model A→ B → C involving an intermediate C is used; reactant is in black, intermediate is in navy and product is in red (top left). Relative contribution of the respective spectral components (or eigen vectors, E.V.) to the overall observed spectrum over the course of time; this represents the time course evolution of the various species involved in the reaction (top right). Plot of residuals (bottom left). Overlay of residuals from a step-wise mechanism (red) and the mechanism involving a single kinetic step (blue, bottom right).

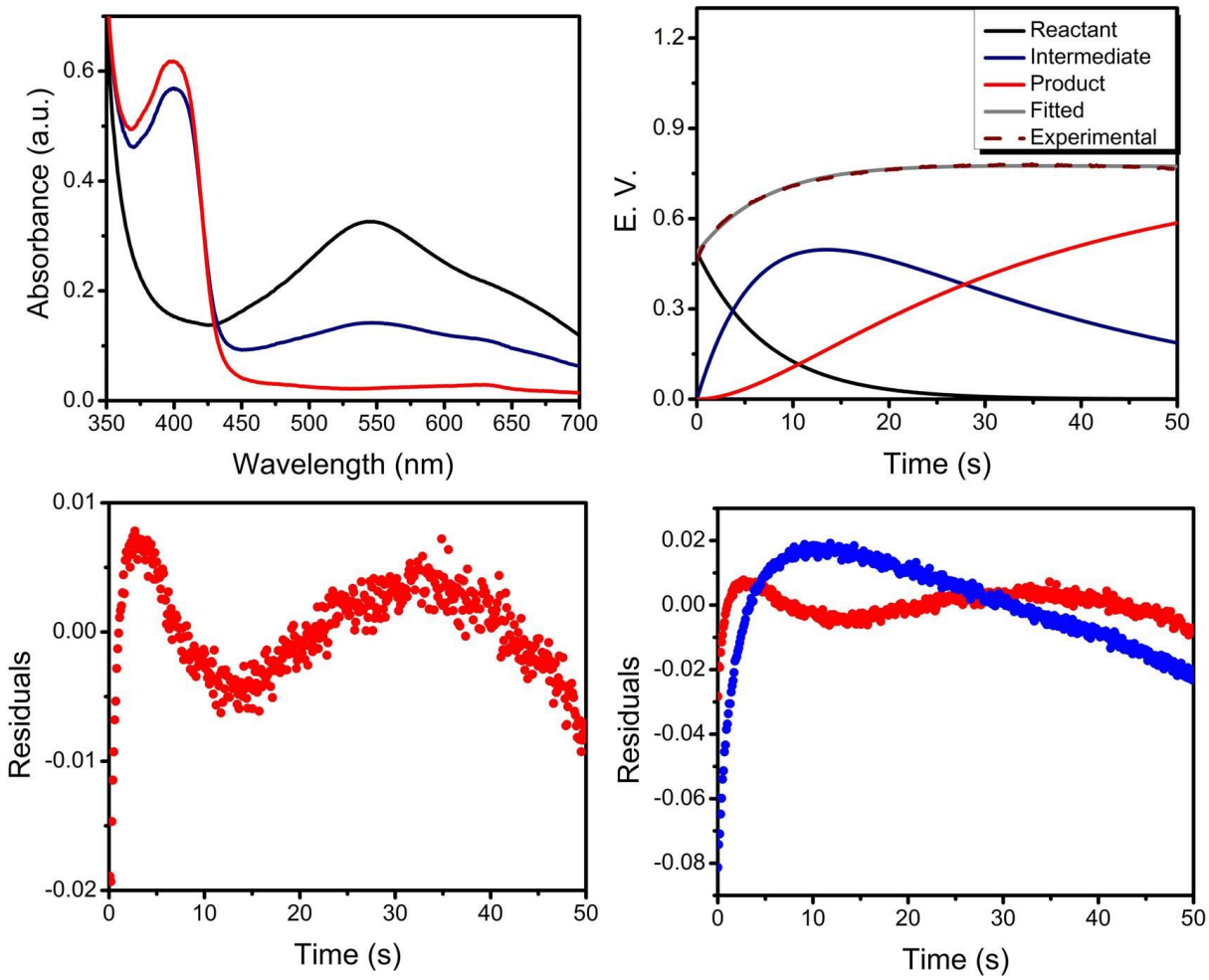

Figure S18. Representative spectral components obtained from the global kinetic analysis using Olis Global Works for *p*-NO_2-phenol reacting with **2a** under pseudo-first order conditions when the kinetic model A→ B → C involving an intermediate C is used; reactant is in black, intermediate is in navy and product is in red (top left). Relative contribution of the respective spectral components (or eigen vectors, E.V.) to the overall observed spectrum over the course of time; this represents the time course evolution of the various species involved in the reaction (top right). Plot of residuals (bottom left). Overlay of residuals from a step-wise mechanism (red) and the mechanism involving a single kinetic step (blue, bottom right).

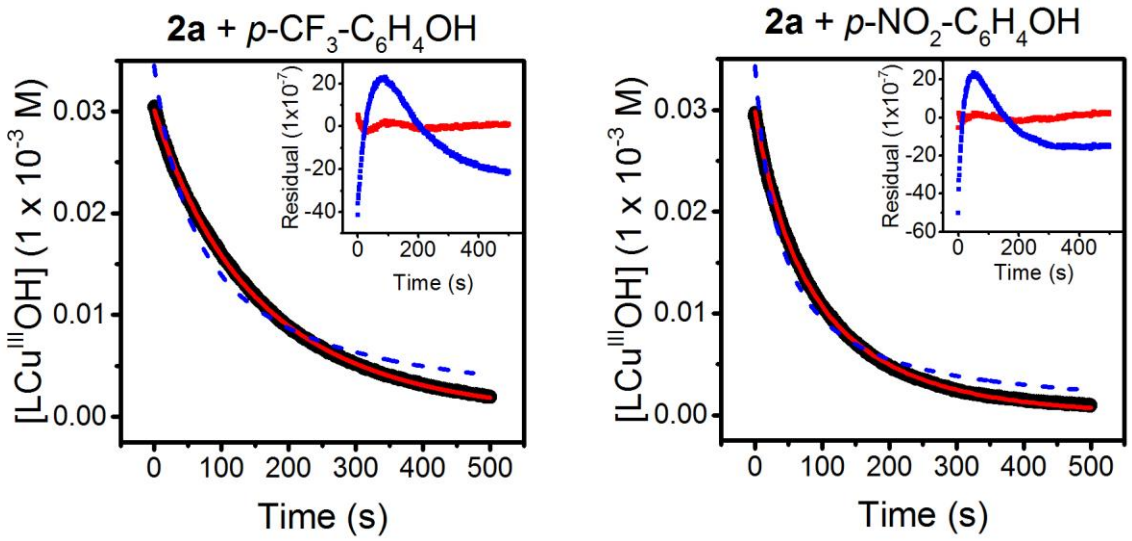

Figure S19. Representative concentration vs. time plots for reactions of **2a** with *p*-CF_3- (left) and *p*-NO_2-phenol, displaying fits to equation S5 (solid red) and S3 (dashed blue), along with the corresponding residual plots (inset). The improved fits to the expanded kinetic model are evident from the residuals.

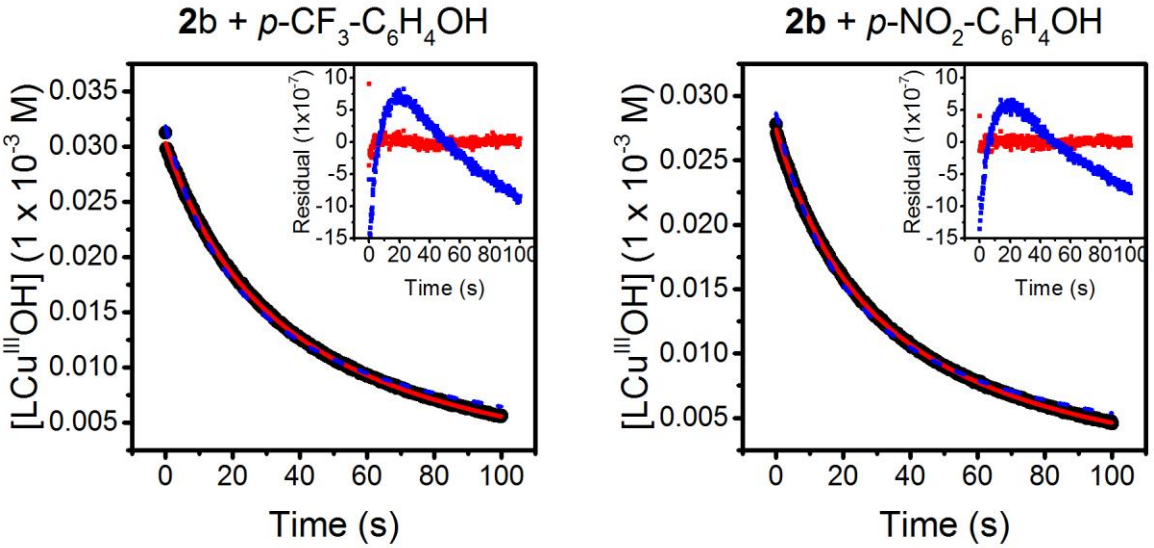

Figure S20. Representative concentration vs. time plots for reactions of **2b** with *p*-CF_3- (left) and *p*-NO_2-phenol, displaying fits to equation S5 (solid red) and S3 (dashed blue), along with the corresponding residual plots (inset). The improved fits to the expanded kinetic model are evident from the residuals.

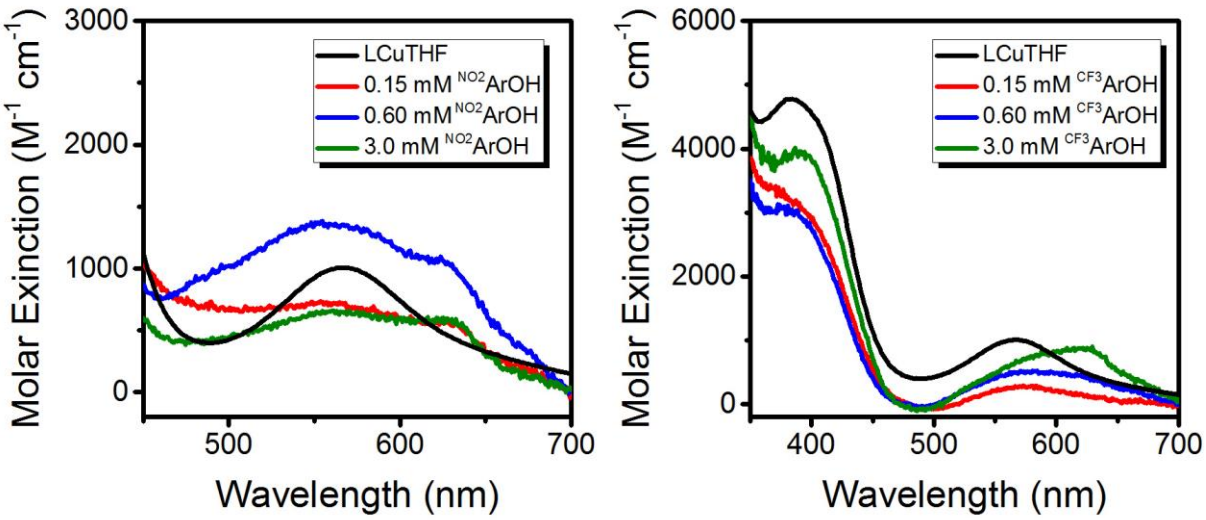

Figure S21. Final decay spectra of pseudo first order stopped-flow reactions between **2a** and ^{NO2}ArOH (left) and ^{CF3}ArOH (right) at the concentrations listed. Molar extinction values were approximated by using the total copper concentration (0.03 mM). The spectra are overlayed with that of the LCu(THF) adduct for comparison.

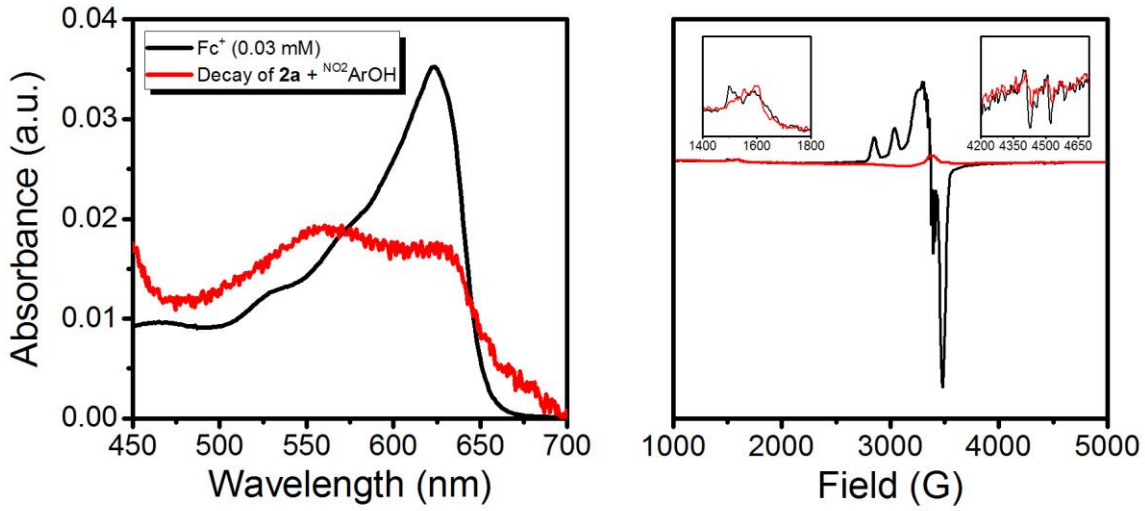

Figure S22. (Left) Overlay of the UV-vis spectra for a 0.03 mM solution of [Fc][BAr$^{F}_{4}$] (black) with the product solution of the reaction between **2a** and 100 eq. of ^{NO2}ArOH (red). (Right) An overlay of the EPR spectra for a 1 mM [Fc][BAr$^{F}_{4}$] solution (red) and the product solution of the reaction of **2a** and 2 eq. of ^{NO2}ArOH (black) with the features due to Fc^{+} shown in the insets.

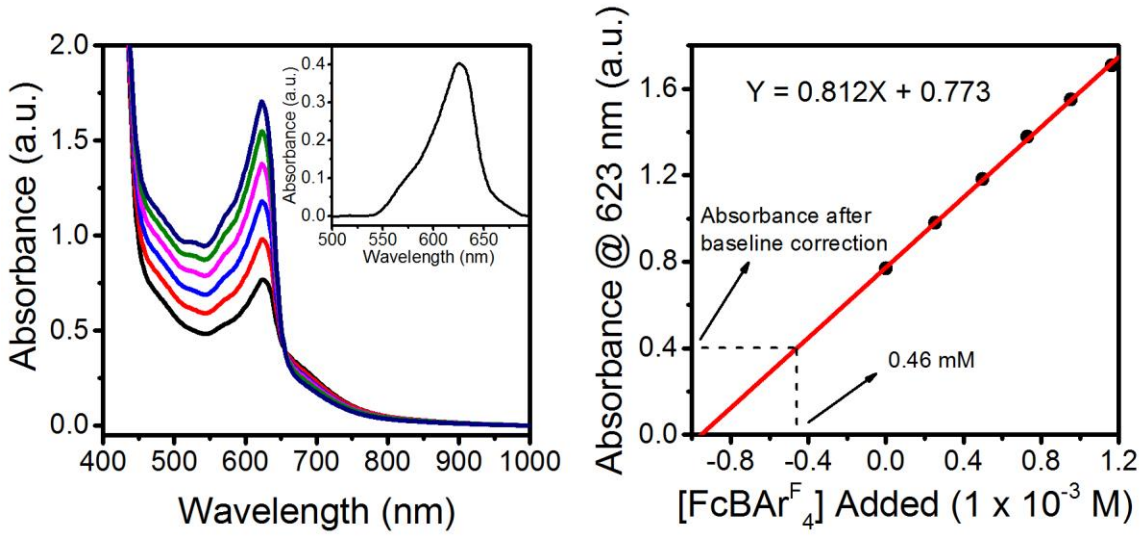

Figure S23. (Left) UV-vis spectrum of the product mixture for the reaction between **2a** and ^{NO2}ArOH in THF at -80 °C (black spectrum; total Cu concentration is 0.5 mM), as well as the corresponding spectra of the same solution upon the addition [Fc][BAr$^F_4$] in of 0.25 eq. (red spectrum), 0.5 eq. (blue spectrum), 0.75 eq (pink spectrum), 1.0 eq. (green spectrum), and 1.25 eq (purple spectrum) increments. The inset shows the original product mixture after baseline correction, which was done to approximate the absorbance solely due to Fc^+ in the product mixture. (Right) Standard addition plot for the addition of [Fc][BAr$^F_4$] to the product mixture corresponding to the UV-vis absorption changes shown in the figure to the left. The absorbance after baseline correction was used to approximate the concentration of Fc^+ in the product mixture from the linear fit.

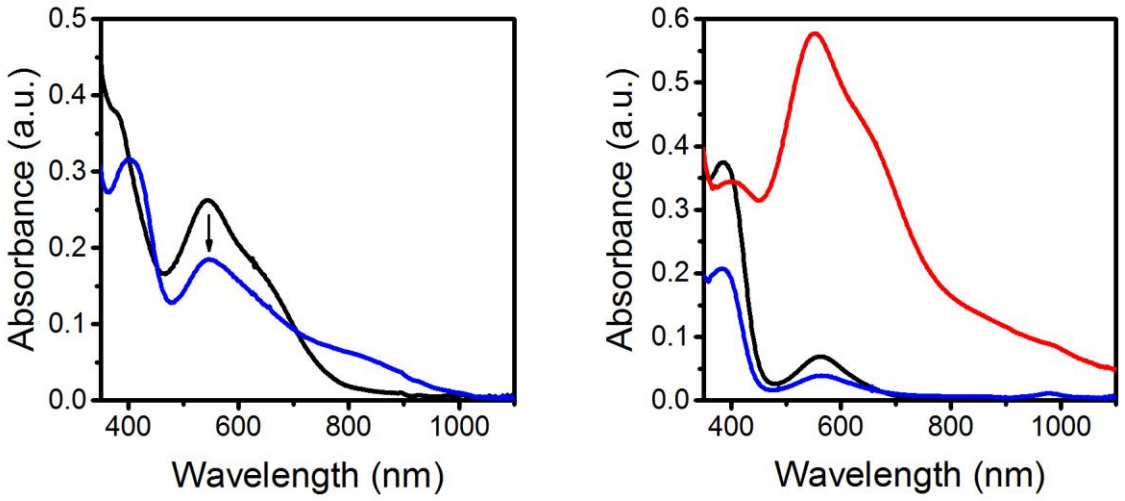

Figure S24. (Left) UV-Vis traces for the reaction between **2a** (black spectrum; generated by addition of 1 eq. of $[C_{12}H_8S_2]PF_6$ to a 0.1 mM solution of **1a** in THF at -80 °C) and 1 eq. of 2,4,6-trimethylpyridinium triflate (blue spectrum) in THF at -80 °C. (Right) UV-vis absorption spectrum of the independently generated $[LCu(OH_2)]^+$ intermediate **4a**, formed by the addition of 1 eq. of $[C_{12}H_8S_2]PF_6$ oxidant to a 0.1 mM solution of $LCu^{II}(THF)$ dissolved in wet Acetone (red) at -80 ºC. The starting spectra of LCu(THF) in dry and wet acetone are shown in black and blue, respectively.

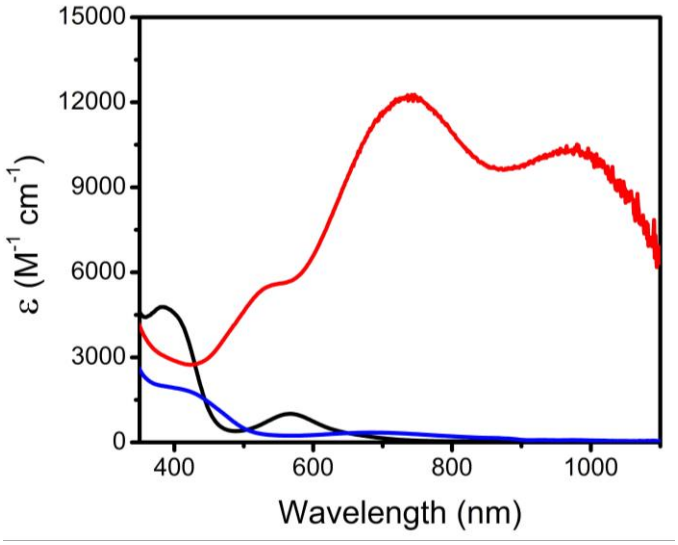

Figure S25. UV-vis absorption spectra of $LCu^{II}(THF)$ in THF (black), $[LCu^{III}(THF)]^+$ in THF generated by addition of 1 eq. of $[C_{12}H_8S_2]PF_6$ (red), and the corresponding decay spectrum of the oxidized species upon warming up to room temperature (blue). All spectra were recorded at -80 ºC.

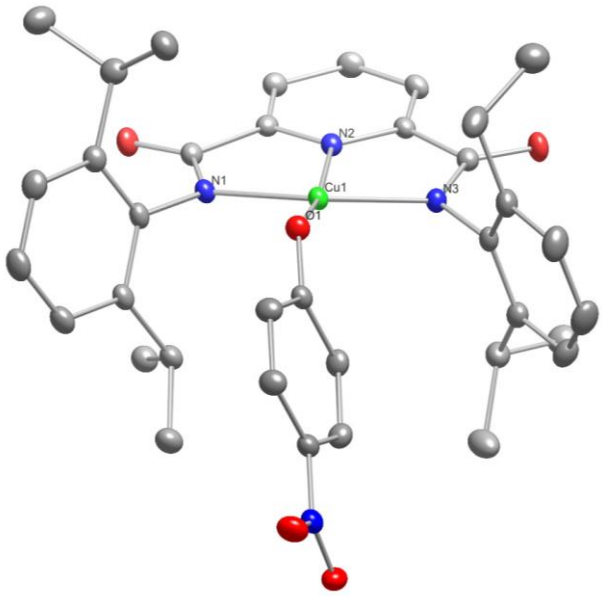

Figure S26. Crystal structure of $[Bu_4N][LCu^{II}OAr^{NO2}]$ with thermal ellipsoids drawn at 50% probability. Green, blue, red, and grey atoms represent Cu, N, O, and C, respectively. H-atoms, counter-ion, and solvent molecules omitted for clarity.

Table S4. Crystal data and structure refinement for 16070_0ma_a.

Identification code	16070_0ma_a	
Empirical formula	C57 H87 Cu N5 O6	
Formula weight	1001.85	
Temperature	293(2) K	
Wavelength	1.54178 Å	
Crystal system	Triclinic	
Space group	P-1	
Unit cell dimensions	a = 12.6607(6) Å	α = 101.482(3)°
	b = 15.4354(7) Å	β = 112.975(2)°
	c = 16.1838(9) Å	γ = 93.732(2)°
Volume	2817.6(2) $Å^3$	
Z	2	
Density (calculated)	1.181 Mg/m^3	
Absorption coefficient	0.947 mm^{-1}	
F(000)	1082	
Crystal color, morphology	Yellow-green with olive notes, block	
Crystal size	0.2 x 0.1 x 0.1 mm^3	
Theta range for data collection	3.058 to 79.889°	
Index ranges	$-16 \le h \le 15$, $-17 \le k \le 19$, $-20 \le l \le 20$	
Reflections collected	73182	
Independent reflections	12061 [R(int) = 0.0400]	
Observed reflections	10564	
Completeness to theta = 67.679°	99.6%	
Refinement method	Full-matrix least-squares on F^2	
Data / restraints / parameters	12061 / 0 / 636	
Goodness-of-fit on F^2	1.025	
Final R indices [I>2sigma(I)]	$R1$ = 0.0408, $wR2$ = 0.0983	
R indices (all data)	$R1$ = 0.0478, $wR2$ = 0.1036	
Extinction coefficient	n/a	
Largest diff. peak and hole	0.557 and -0.459 $e.Å^{-3}$	

$R_{int} = \Sigma\ |F_o^2 - < F_o^2 >| / \Sigma|F_o^2|$, $R_1 = \Sigma||F_o|-|F_c|| / \Sigma|F_o|$, $wR2 = [\Sigma[w(F_o^2-F_c^2)^2] / \Sigma\ [w(F_o^2)^2]]^{1/2}$

where $w = q / [\sigma^2(F_o^2) + (a*P)^2 + b*P + d + e*\sin(\theta)]$,GooF = $S = [\Sigma[w(F_o^2-F_c^2)^2] / (n-p)]^{1/2}$

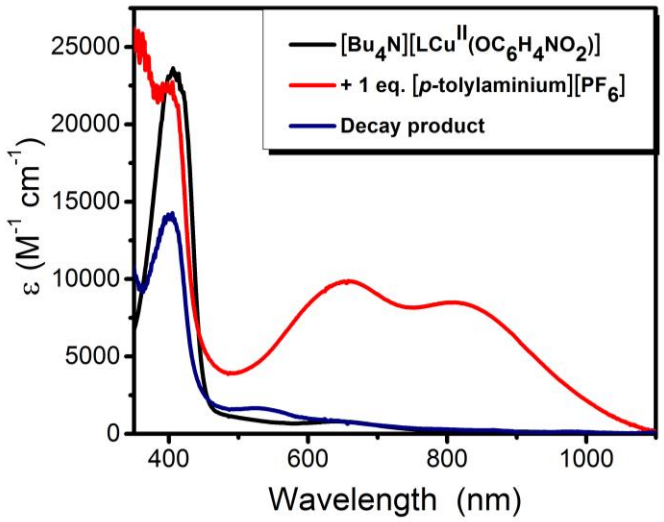

Figure S27. UV-Vis absorption spectra of a THF solution of $[Bu_4N][LCu^{II}OAr^{NO2}]$ (black), after the addition of 1 eq. of $[(p\text{-tolyl})_3N]PF_6$ (red), and the final decay spectrum of the oxidized species after warming up to room temperature (blue). All spectra were recorded at -80 °C.

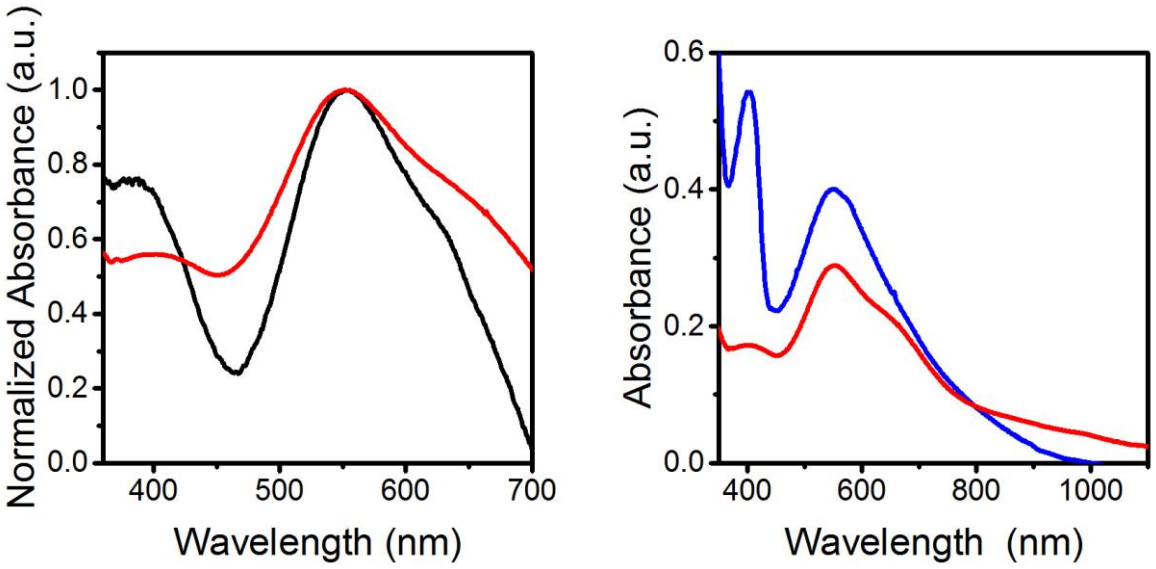

Figure S28. (Left) Overlay of the UV-vis spectra corresponding to the intermediate identified from global fitting of the reaction between **2a** (from stopped-flow studies, generated by treatment of **1a** with 1 eq. of Fc^+) and ^{NO2}ArOH (black) and the experimentally measured spectrum of $[LCu^{III}(OH_2)]^+$ (**4a**) generated by treatment of LCu(THF) in wet acetone with 1 eq. of $[C_{12}H_8S_2]PF_6$ at -80 ºC (red). The spectra are normalized. (Right) Overlay of the spectrum of the intermediate in the reaction of **2a** with ^{NO2}ArOH using $[(p\text{-tolyl})_3N]PF_6$ as the oxidant (blue) and the spectrum of $[LCu^{III}(OH_2)]^+$ (**4a**) generated by treatment of LCu(THF) in wet acetone with 1

eq. of $[C_{12}H_8S_2]PF_6$ at -80 ºC (red). Both reactions are performed at a 0.05 mM concentration of the copper complex.

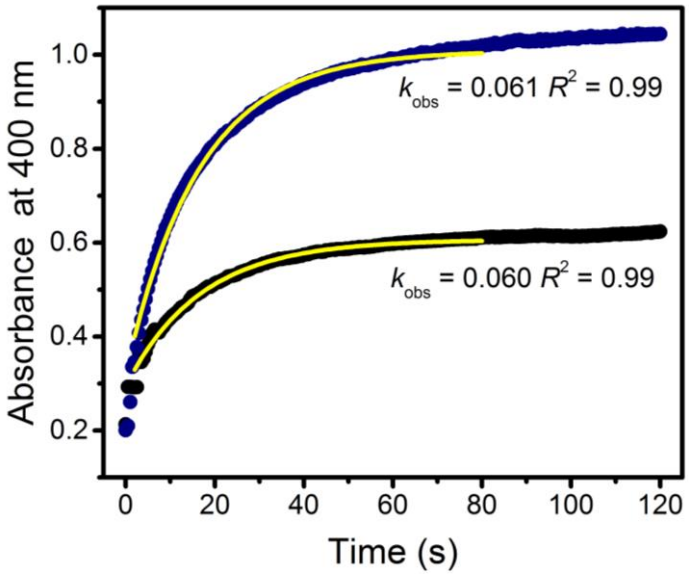

Figure S29. Representative single exponential fits (yellow) to the absorbance at 400 nm vs. time for reactions of **2a** (0.05 mM concentration) with ^{NO2}ArOH (5 eq.) using 1 eq. of $[Fc][BAr^F{}_4]$ (blue) or $[(p\text{-tolyl})_3N]PF_6$ (black) as the oxidant.

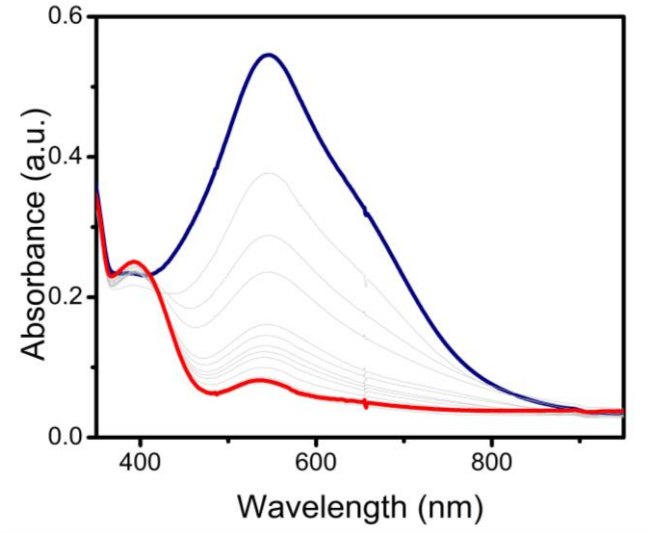

Figure S30. UV-Vis traces on treatment of **2a** (generated by oxidation of **1a** with $(p\text{-tolyl})_3NPF_6$)) with 2 eq. of *p*-cresol monitored in THF at -80 °C.

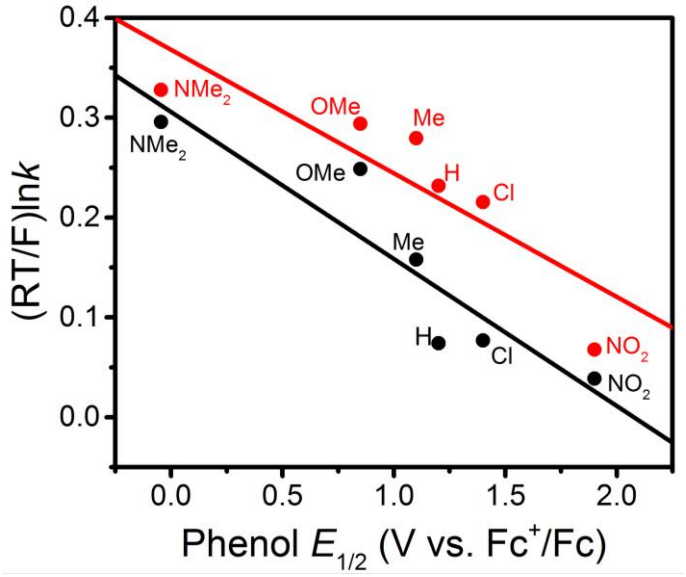

Figure S31. Plots of (RT/F)ln$k$ vs. Phenol $E_{1/2}$ for reactions of **2a** (black) and **2b** (red) with ^{X}ArOH (X labeled). Linear fits have slopes of -0.17 (R^2 = 0.80) and -0.12 (R^2 = 0.70) for the reactions with **2a** and **2b**, respectively.

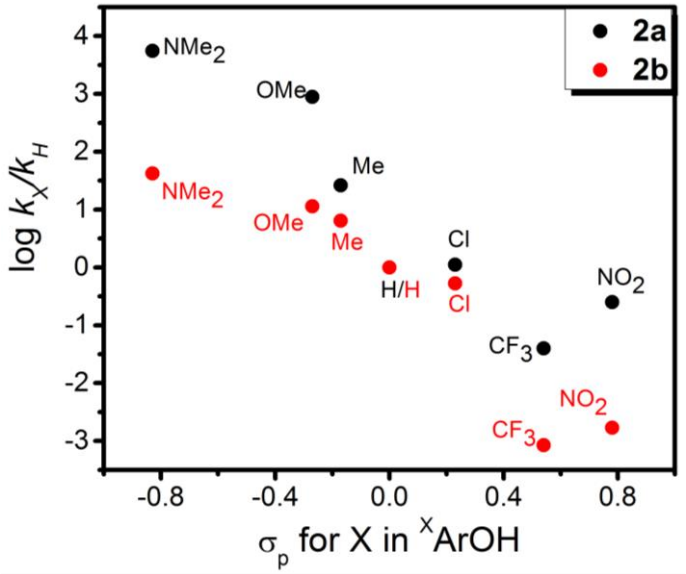

Figure S32. Hammett plots for reactions of **2a** (black) and **2b** (red) with ^{X}ArOH (X labeled).

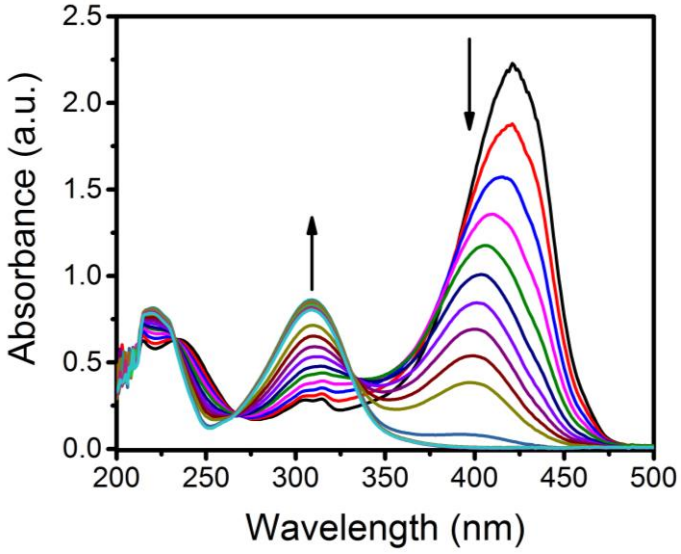

Figure S33. UV-vis titration of a 0.1 mM solution of [Bu4N][^{NO2}ArO] (black spectrum) with the weak acid Et_3NHOTf (2 mM). Each additional spectrum shows the conversion of $^{NO2}ArO^-$ to ^{NO2}ArOH and corresponds to a 0.05 mL addition of Et_3NH^+.

Table S5. Titration data for the pK_a determination of ^{NO2}ArOH in THF corresponding to Figure S29.

$[Et_3NH^+]_{Total}$ (M)[a]	$[^{NO2}ArO^-]_{eq}$ (M)[b]	$[^{NO2}ArOH]_{eq}$ (M)[c]	$[Et_3NH^+]_{eq}$ (M)[d]	$[Et_3N]_{eq}$ (M)[c]	K_{eq}	pK_{eq}	pK_a[e]
0	1.01×10^{-4}	0	0	0	-	-	-
4.65×10^{-5}	8.55×10^{-5}	1.59×10^{-5}	3.06×10^{-5}	1.59×10^{-5}	9.62×10^{-2}	1.02	13.88
9.09×10^{-5}	7.03×10^{-5}	1.52×10^{-5}	7.57×10^{-5}	1.52×10^{-5}	4.34×10^{-2}	1.36	13.54
1.33×10^{-5}	5.75×10^{-5}	1.27×10^{-5}	1.21×10^{-4}	1.27×10^{-5}	2.34×10^{-2}	1.63	13.27
1.74×10^{-4}	5.01×10^{-5}	7.45×10^{-5}	1.66×10^{-4}	7.45×10^{-5}	6.67×10^{-2}	2.18	12.72
2.13×10^{-4}	3.62×10^{-5}	1.39×10^{-5}	1.99×10^{-4}	1.39×10^{-5}	2.68×10^{-2}	1.57	13.33
2.50×10^{-4}	2.79×10^{-5}	8.24×10^{-6}	2.42×10^{-4}	8.24×10^{-6}	1.01×10^{-2}	2.00	12.90
2.86×10^{-4}	2.13×10^{-5}	6.60×10^{-6}	2.79×10^{-4}	6.60×10^{-6}	7.31×10^{-3}	2.14	12.76
3.20×10^{-4}	1.56×10^{-5}	5.76×10^{-6}	3.14×10^{-4}	5.76×10^{-6}	6.76×10^{-3}	2.17	12.73
3.53×10^{-4}	1.04×10^{-5}	5.15×10^{-6}	3.48×10^{-4}	5.15×10^{-6}	7.30×10^{-3}	2.14	12.76
3.85×10^{-4}	5.97×10^{-6}	4.47×10^{-6}	3.80×10^{-4}	4.47×10^{-6}	8.79×10^{-3}	2.06	12.84
4.15×10^{-4}	-	3.98×10^{-6}	4.11×10^{-4}	3.98×10^{-6}	1.93×10^{-2}	1.72	13.18
						Average	**13.1 ± 0.4**

[a] Based on the total amount of Et3NH$^+$ added. [b] Determined from the raw absorbance value at the λ_{max} using the known value of ε for the feature at ~ 400 nm. [c] Taken as the concentration change in $[^{NO2}ArO^-]_{eq}$ upon addition of Et_3NH^+. [d] Taken as the difference between $[Et_3NH^+]_{Total}$ and $[^{NO2}ArOH]_{eq}$. [e] Taken as the difference between the pK_a of Et_3NH^+ in THF (14.9) and pK_{eq}.

Notes and References

1 P. J. Donoghue, J. Tehranchi, C. J. Cramer, R. Sarangi, E. I. Solomon and W. B. Tolman, *J. Am. Chem. Soc.*, 2011, **133**, 17602-17605.

2 D. Dhar, G. M. Yee, A. D. Spaeth, D. W. Boyce, H. Zhang, B. Dereli, C. J. Cramer and W. B. Tolman, *J. Am. Chem. Soc.*, 2016, **138**, 356-368.

3 J. L. Bras, H. Jiao, W. E. Meyer, F. Hampel and J. A. Gladysz, *J. Organomet. Chem.*, 2000, **616**, 54−66.

4 L. Eberson and B. Larsson, *Acta Chem. Scand., Ser. B*, 1987, **41**, 367-378.

5 C. C. Ferrón, M. Capdevila-Cortada, R. Balster, F. Hartl, W. Niu, M. He, J. J. Novoa, J. T. López Navarrete, V. Hernández and M. C. Ruiz Delgado, *Chem. –Eur. J*, 2014, **20**, 10351-10359.

6 K. L. Seim, A. C. Obermeyer and M. B. Francis, *J. Am. Chem. Soc.*, 2011, **133**, 16970–16976.

7 Olis GlobalWorks 3D Analysis Software. For illustrative references see (a) R. J. DeSa, I. B. C. Matheson, *Meth. Enzymol.*, 2004, **384**, 1-8. (b) E. R. Henry, J. Hofrichter, *Meth. Enzymol.*, 1992, **210**, 129-192. (c) N. Sreerama, S. Y. Venyaminov and R. W. Woody, *Anal. Biochem.*, 2001, **299**, 271-274.

8 Since only the first 5-10% of the data are used in the fitting process (method of initial rates), and given that the absorbances of the products in this case are small, we make the assumption that the contribution to the absorbance from the products is negligible at the start of the reaction.

9 For representative references, see (a) D. Lavabre, V. Pimienta, G. Levy, and J. C. Micheau. *J. Phys. Chem.* 1993, **97**, 5321-5326. (b) S. Lowell. *J. Chem. Educ.*, 1965, **42**, 552. (c) J. H.

Espenson, *Chemical Kinetics and Reaction Mechanisms*, McGraw-Hill Companies, New York, Second Edition, 2002.

10 D. Dhar and W. B Tolman, *J. Am. Chem. Soc.*, 2015, **137**, 1322-1329.

11 Furthermore, the global fits of the pseudo first-order data indeed show that the reactions of **2a/b** with ^{NO2}ArOH and ^{CF3}ArOH fit better to a 2-step kinetic model. While it is likely that expanding the rate law in equation S5 to include these additional mechanistic pathways would result in better fits, we feel that this would be relying too heavily on the kinetic modeling. Thus, to avoid over modelling, we have refrained from including any additional kinetic pathways.

12 V. W. Manner, T. F. Markle, J. H. Feudenthal, J. P. Roth, and J. M. Mayer, *Chem. Commun.*, 2008, 256-258.

13 (a) D. W. Snelgrove, J. Lusztyk, J. T. Banks, P. Mulder and K. U. Ingold, *J. Am. Chem. Soc.*, 2001, **123**, 469-477. (b) M. F. Nielsen and K. U. Ingold, *J. Am. Chem. Soc.*, 2006, **128**, 1172-1182. (c) M. H. Abraham, P. L. Grellier, D. V. Prior, P. P. Duce, J. J. Morris and P. J. Taylor, *J. Chem. Soc., Perkin Trans. 2*, 1989, 699-711.